國立臺灣大學工學院機械工程研究所

碩士論文

Graduate Institute of Mechanical Engineering

College of Engineering

National Taiwan University

Master Thesis

利用旋轉塗佈法製備還原氧化石墨烯適體生物感測器

應用於心臟 Troponin-I 檢測之研究

Research of reduced-graphene-oxide-based cardiac

Troponin-I biosensor fabricated by spin-coated method

陳俞齊

Yu-Chi Chen

指導教授：施文彬 博士

Advisor: Wen-Pin Shih, Ph.D.

中華民國 105 年 7 月

July, 2016

國立臺灣大學碩士學位論文
口試委員會審定書

利用旋轉塗佈法製備還原氧化石墨烯適體生物感測器應用於心臟 Troponin-I 檢測之研究
Research of reduced-graphene-oxide-based cardiac Troponin-I biosensor fabricated by spin-coated method

本論文係陳俞齊君（R03522502）在國立臺灣大學機械工程學系完成之碩士學位論文，於民國 105 年 7 月 20 日承下列考試委員審查通過及口試及格，特此證明

口試委員：

＿＿＿＿＿＿＿＿＿＿＿＿　（簽名）
（指導教授）

＿＿＿＿＿＿＿＿　　＿＿＿＿＿＿＿＿

＿＿＿＿＿＿＿＿　　＿＿＿＿＿＿＿＿

系主任　＿＿＿＿＿＿＿＿＿＿　（簽名）

致謝

在台大兩年的研究所生涯很快就過了，在此要感謝所有幫助過我的教授、學長與同學，讓我能夠順利地完成碩士學位。特別要感謝指導教授施文彬，感謝施老師對我兩年來的栽培，每週的會議也讓我能夠一步一步地進行研究，也感謝老師提供充分的資源，讓我能無後顧之憂地學習與做實驗，在老師的指導下，學到了研究應有的態度與方法，施老師有創意且有前瞻性的眼光，讓我受益良多。還要感謝中興大學生機系蔡燿全教授，蔡教授給予我研究以及論文相當多的幫助。

感謝實驗室的學長姐和學弟:承俊、品淳、梁道、仁傑、富城、承義、期宇、淳右、柏安、恆嘉、瑞鴻、彥廷、明華與胤禎，提供許多寶貴的研究經驗與建議，特別要感謝期宇學長以及承俊學長，他們的帶領讓我在研究過程能夠更加順利。很開心能跟同屆的紹傑、彥安、瑋傑一起度過研究所的兩年，彼此互相鼓勵，一起努力。感謝 Mandy 在我失落的時候幫我打氣，讓我能夠撐下去。也感謝台大奈米機電系統研究中心，提供良好的儀器使我研究能夠順利完成。還要感謝電機系林致廷老師實驗室提供儀器的協助。此外，很感謝在台大陪伴我的同學們，景棠、君彥、百育、壞正、柏崴、耀德、千豪、暄明，在各位的陪伴下，一起完成了碩士學位。還有北科大的研究夥伴們，昱仁學長、懷緯學長以及杰倫，在每個月的計畫會議互相討論和分享研究過程。

最後要感謝家人的支持與陪伴，體諒我回台北的這兩年來，很少時間在家裡好好陪伴他們。最後期盼自己能在未來的路上保持樂觀且上進的態度面對一切，為屬於自己的一片天努力，並有所成就將來回報父母與一路上曾經幫助過我的貴人。

<div align="right">
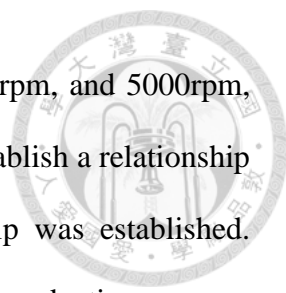
陳俞齊 Aug. 2016

</div>

中文摘要

　　本論文以開發心臟病量測晶片為背景，利用旋轉塗佈法（Spin-coating method）在量測晶片上製作還原氧化石墨烯(Reduced graphene oxide)薄膜，以其用來當作感測區材料。臨床上對於急性冠心症(acute coronary syndrome, ACS)的診斷為症狀評估、心電圖的缺氧變化以及心肌酶濃度升高，而心肌生物標記(Cardiac biomarker)的濃度在心肌受損初期即會微量提升，因此只要提早偵測到生物標記的濃度變化，將可及時對病患做緊急治療。本論文所屬計畫致力於開發一生物感測晶片，期望能使用二維材料-石墨烯(Graphene)來當作感測區，以達到使用方便、檢測快速、效能穩定、價格便宜的效果，因此將著重於製備石墨烯薄膜的方法以及其均勻性的控制，以能夠成為商品及量產為目標。利用石墨烯作為感測區的方式已有許多文獻提出，然而多以化學氣相沉積法(chemical vapor deposition, CVD)來製備，再藉由濕式轉印方式將石墨烯轉移至感測晶片上，此轉印的過程中，通常會造成石墨烯機械應力的拉扯以及損毀，因此本論文使用石墨烯氧化物以及旋轉塗佈法來製備石墨烯氧化物薄膜，以達到更為均勻之石墨烯薄膜。在本論文中，首先將石墨烯氧化物分散於甲醇與水的混和分散液中，利用食人魚洗劑(Piranha solution)以及半胱胺(cysteamine)對基材二氧化矽(SiO_2)以及金電極(Au)進行親疏水改質，藉由親疏水性的改變，石墨烯氧化物薄膜的覆蓋率可從 36% 提升至 100%。再使用旋轉塗佈法將石墨烯氧化物旋塗在改質過後的晶片表面，並藉由白光干涉儀(Optics-Type surface analyser)可得知當轉速為每分鐘 2000、3000、4000 以及 5000 轉時，石墨烯氧化物厚度為 14.4 nm、10.2 nm、7.2 nm 以及 6.6 nm，經由與 Washo's 與 Meyerhofer's 模型比較膜厚與轉速之間的關係，可得膜厚與轉速成-0.905 次方關係。最後將石墨烯氧化物薄膜泡入抗壞血酸(L-Ascorbic acid)水溶液中進行還原，並利用拉曼光譜儀(Raman spectrometer)中 D band 與 G band 的比例變化來證實還原氧化石墨烯的氧化程度，其中 I_D/I_G 還原前為 0.93 還原後為 1.05，其中以每分鐘 5000 轉時重複旋塗 3 次擁有最好的電阻穩定性，此時平均電阻值為 0.25 Ω，誤差除以平均值為4.3%。

關鍵字：急性冠心症、生物標記、生物感測器、旋轉塗佈法、石墨烯、石墨烯氧化物、還原氧化石墨烯、接觸角、親疏水性改質、拉曼光譜

ABSTRACT
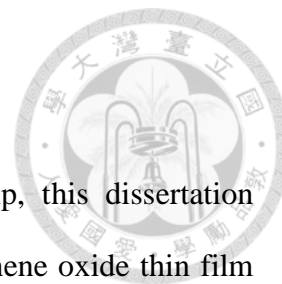
Based on the development of a heart disease detection chip, this dissertation proposed to adopt the spin-coating method to form a reduced graphene oxide thin film as the sensing material on the detection chip. The clinical diagnosis of acute coronary syndrome, ACS, is based on symptom assessment, signs of oxygen deprivation on the electrocardiogram (ECG), and increase in the myocardial enzyme concentration. Because the concentration of cardiac biomarkers is increased in the early stage of myocardial damage, the early detection and subsequent emergency treatment of patients is possible. This dissertation is a part of a larger project that is targeted at developing a biosensor chip using a two dimensional material, graphene, as the detector region in order to realize a final product that is convenient, rapid, stable, and cost-effective. Therefore, this study is emphasized on the graphene thin film preparation method as well as the uniformity control with the goal of developing and mass producing for an actual product. While several studies have already proposed to employ the graphene as the sensor region material, most teams used the method of chemical vapor deposition (CVD) followed by subsequent transferring via wet-printing to the sensor region of the chip. However, during the transfer process, defects may occur resulting from the mechanical residual stress in the graphene's structure. Thus, this study employed the spin-coating method to prepare a graphene oxide (GO) thin film that was highly uniform. Briefly, GO was first dispersed in a solution containing water and methanol. On the side, a piranha solution and cysteamine solution were used to modify the SiO_2 and Au electrode surface for the hydrophilicity. By increasing the hydrophilicity of the substrate, the coverage of the GO thin film increased from 36% to 100%. Then the spin-coating method was used to cover the GO onto the modified chips. As determined using the Optics-Type surface analyser, the thickness of the GO film was 14.4 nm, 10.2

nm, 7.2 nm, and 6.6 nm at spin rate of 2000 rpm, 3000 rpm, 4000rpm, and 5000rpm, respectively. After adopting Washo's and Meyerhofer's models to establish a relationship between film thickness and spin rate, a -0.905 power relationship was established. Lastly, the GO film was soaked in an $_L$-Ascorbic acid solution for the reduction process. The reduction level was determined by Raman spectroscopy through calculating the change in the ratio of the D band and the G band. Wherein, I_D/I_G was 0.93 before reduction and 1.05 after reduction. The highest resistance stability was achieved by coating at 5000 rpm for three times. The resultant mean resistance value was 0.25Ω and the standard deviation/mean value was 4.3%.

Keywords: Acute coronary syndrome, Biomarker, Biodetector, Spin-coating, Graphene, Graphene oxide, Reduced graphene, Contact angle, Hydrophilic modification, Raman spectroscopy.

SYMBOL TABLE

A   Constant term of experimental eq. 2.15

B   Exponential term of experimental eq. 2.15

h_0 The end of spin-up stage thickness

h_t Final film thickness

q The radial flow

r The radial distance from the z axis on the rotation disk

z The signed distance from the plane of rotation disk

ω Angular velocity

ω_f Final spin rate

θ The angle between the reference direction on rotation disk

η Absolute viscosity

ρ Fluid density

v Velocity in the direction of r

ρ_0 The initial value of ρ

ϕ The evaporation rate of the solvent
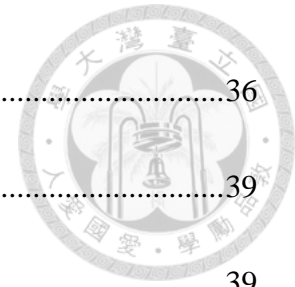
CONTENTS

LIST OF FIGURES

x

LIST OF TABLES

Chapter 1 Introduction

1.1 Background

1.1.1 Acute coronary syndrome

There are more and more people suffering from cardiovascular disease, generally referred to conditions that involve narrowed or blocked blood vessels that can lead to a heart attack, chest pain (angina) or stroke [1]. People nowadays have increasing probability of having cardiovascular disease with increasing salt or, fat consumption. Acute coronary syndrome (ACS), clinical presentation of myocardial ischemia, occurs when heart muscles lack of oxygen because of narrowed or blocked blood vessel. There were more than 1.1 million patients with acute coronary syndrome (ACS) in U.S in 2010 [1], and about 114,000 people go to hospital because ACS in UK each year [2]. ACS can be divided into ST-segment elevation myocardial infarction (STEMI), non–ST-segment elevation myocardial infarction (NSTEMI) and unstable angina according to its different symptoms, electrocardiography (ECG) and enzymes concentration. In clinical, many kinds of ACS's examination were proposed including electrocardiography and different kinds of enzymes. In particular, enzymes detection spends a lot of time and the patient suffered ACS must be sent to the hospital to do such examination before being arranged to the next treatment. However, it is always very urgent for an ACS patient to arrive at hospital. Therefore, more and more laboratories

aim to develop a biosensors to detect the enzymes concentration in blood quickly and easily.

1.1.2 Cardiac muscles and troponin

Cardiac muscle is one of three major muscles in human body; the others are skeletal and smooth muscles. Cardiac muscle can not be controlled by brain, so called involuntary muscle, but can coordinate contracts for heart to pump blood to the whole body for oxygen supply. Like most other tissues in body, cardiac muscles need blood to deliver oxygen and nutrients and to remove waste products. The artery which supplies blood to cardiac muscles is called coronary artery. If the coronary arteries became narrowed or blocked, the cardiac muscles damaged and lost the ability to pump blood
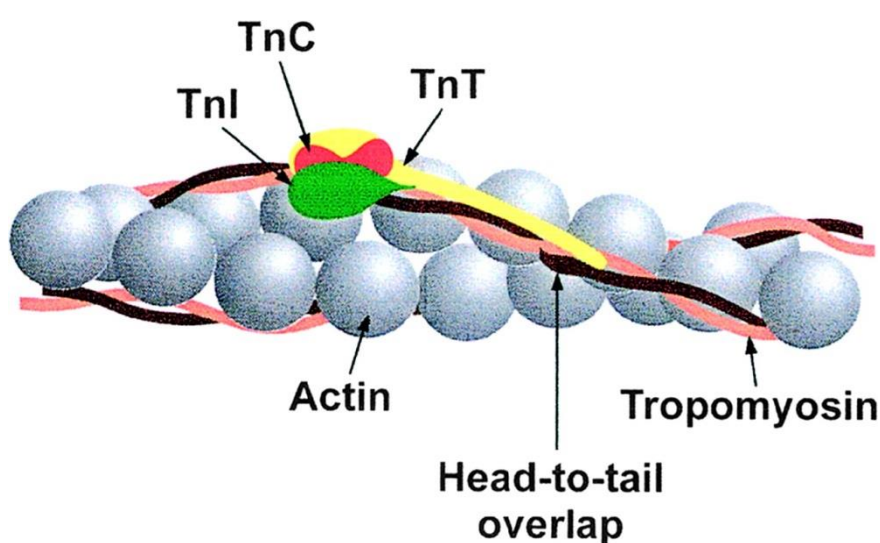
Figure 1-1 Proteins comprise cardiac myofilaments [3].

2

efficiently due to the lack of oxygen supplied. Furthermore, sever blockage in coronary artery will lead to cardiac muscles necrosis.

Cardiac troponins include three different proteins: troponin-I (TnI), troponin-T (TnT), and troponin-C (TnC). As shown in Figure 1-1 [3], all of them act as key roles in cardiac muscle contraction. They act together as a complex in inhibiting the binding of myosin to actin strands. TnT acts as a linker between troponin complex and myosin, TnI blocks the binding site between myosin and actin; TnC binds with calcium ion and then performs conformal change to move TnI away from the binding site. Therefore, the muscles can do contraction.
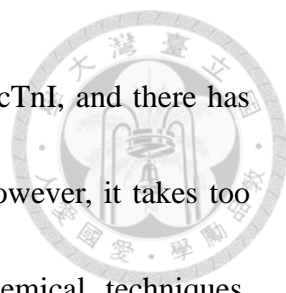
When ACS occurs, cardiac tissue necroses. In this situation, cardiac troponins are released into blood. cTnI has been proved as the standard and an attractive biomarker for presymptomatic diagnosis; it is discriminative from the troponin of skeletal muscle [4]. Figure 1-2 shows the cardiac troponin (cTn) evolution assays and their diagnostic cutoff. The diagnostic cutoff was 1.5 ng/mL at about 7.5 hours after onset of ACS in 1995; it was improved to 0.1 ng/mL at about 4 hours after onset of ACS in 2003; and it was improved to 0.04 ng/mL at about 3.5 hours after onset of ACS in 2007. Therefore, if the limit of detection for cTnI detection can be improved, the ACS could be diagnosed as early as possible so that the patient could be accepted remedy in time.

3
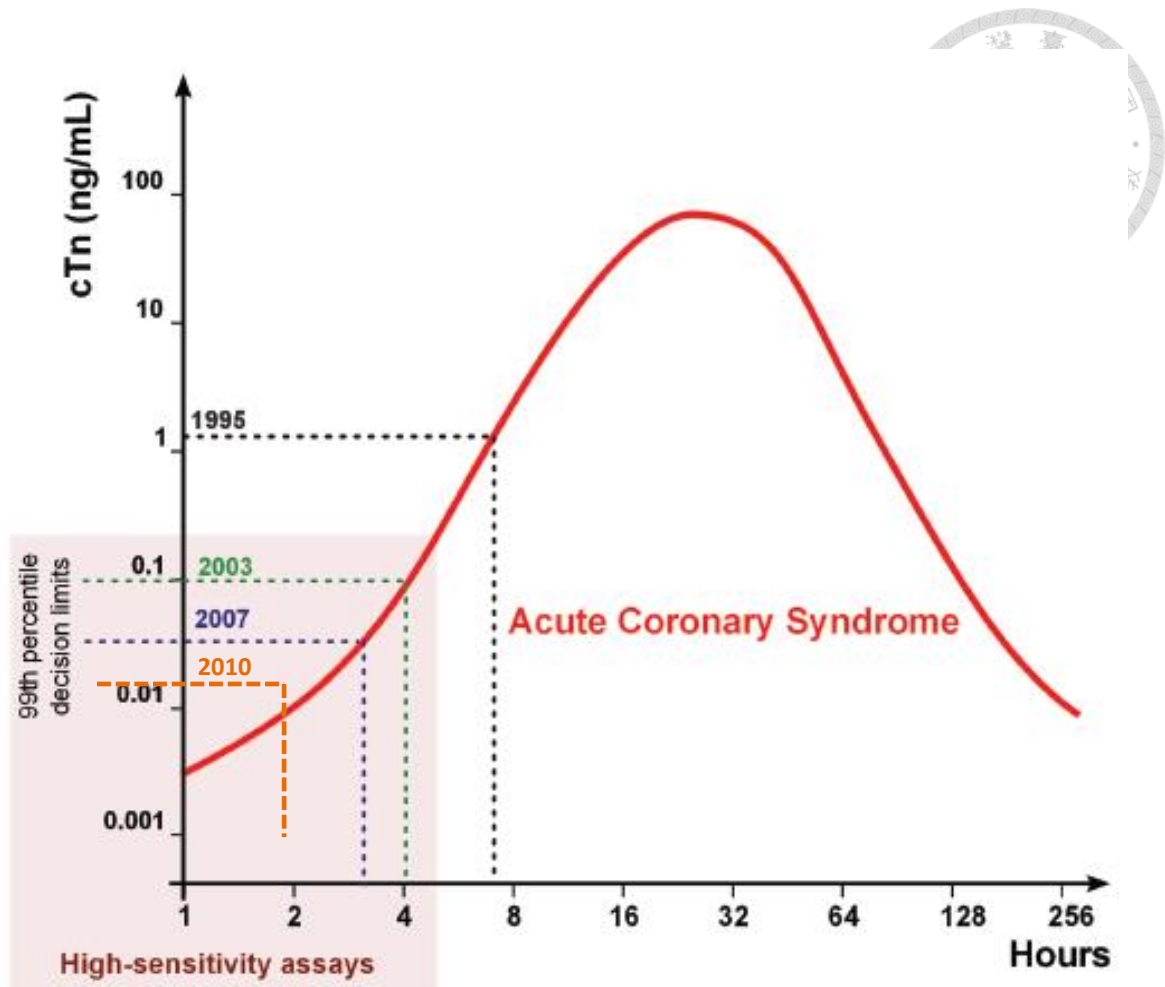
Figure 1-2 Evolution of the cardiac troponin (cTn) assays and their diagnostic cutoff [5].

1.1.3 Tropnin detection

Biosensors are taken as an important role for future medical care system that is looked forward to be available for point-of-care. Therefore, the essentials of biosensors in practical usage are portability, convenient execution, rapid detection, high sensitivity, and low cost [6], [7]. Detection platforms of cTnI biomarkers with various sensing methods have been investigated in last few years. Enzyme-linked immunosorbent assay

4

(ELISA) is the common method to determine the concentration of cTnI, and there has been commercial product with limit of detection at 0.03 ng/mL. However, it takes too much time more than 5 hours of analysis time [8]. Electrochemical techniques, including electrochemical impedance spectroscopy (EIS) [9] and cyclic voltammetry (CV) [10], were reported with limit of detection to be 0.2 ng/mL and 1 ng/mL, respectively. The frequency change due to mass change of the captured cTnI biomarkers on quartz crystal microbalance (QCM) indicated the limit of detection of 0.34 μg/mL [11] . The guided-mode resonance method measures the shift of reflection peak wavelength, and its LOD for cTnI detection was 0.05 ng/mL [12]. The colorimetric method with silver enhanced poly(dimethylsiloxane) (PDMS)-gold nanoparticles (AuNPs) composite film to detect cTnI has the detection limit of 0.01 ng/mL [13]. The principle of surface plasmon resonance (SPR) was applied via red-shift when cTnI biomarkers bind with antibodies which were conjugated in gold nano-rods solution [14], [15]. The peptide-based biosensor with gold nanoparticles for intensity amplification utilized electrogenerated chemiluminescence (ECL) to reach the limit of detection of 0.1 ng/mL [16]. According to these researches, the limit of detection could improve to be 0.01 ng/mL in 2010. Back to Figure 1-2, ACS could be diagnosed 2 hours later after the onset of AMI using these mentioned methods. However, these detecting techniques need long reaction time or expensive analysis equipment. Some of them even have difficult

5

handling process. Conversely, the direct detection of protein biomarkers with field effect

transistor (FET) could be a promising easy-use biosensor if integrated with circuitry and

microfluidics [17], [18].

Table 1-1 Comparison in cardiac troponin-I biosensors

Sensor-type	Limit of detection	reference
Enzyme-linked immunosorbent assay (ELISA)	0.03 ng/mL	Commercial Product [8]
Cyclic voltammetry (CV)	0.2 ng/mL	2013 [10]
Electrochemical impedance spectroscopy (EIS)	0.2 ng/mL	2012 [9]
Quartz crystal microbalance (QCM)	0.34 µg/mL	2010 [11]
Silver enhanced colorimetric	0.01 ng/mL	2010[13]
Guided-mode resonance (GMR)	0.05 ng/mL	2010[12]
Surface plasmon resonance (SPR)	0.07 ng/mL	2011[14],[15]
Electrogenerated chemiluminescence (ECL)	0.1 ng/mL	2014[16]

1.2 Biosensors

1.2.1 Concept of biochip

Biosensors have been developed four decades, the enzyme electrode was the earliest development by Clark and Lyon. They modified the electrode by glucose oxidase, and defined the concentration of glucose by detecting oxygen consumption with galvanometer [19]. In 1967, Updisk and Hicks successfully development a blood glucose monitors with DO (dissolved oxygen) electrode detection technology [20]. In this method, enzyme glucose was immobilized on the electrode by polyacrylamide. Yellow Spring Instrument Company commercialized this concept. They produced and packaged it into a known blood glucose tester (glucosemeter) in 1979, which was the first generation biosensor at medical examination market.

Saltzgaber and his colleagues [20] demonstrated that when DNA was affixed to the channel surface, both the streaming current and the amplitude were altered. Thus, such strategy could be used to detect the presence of DNA. Using the similar concept, Ueda and Martins proposed micro-channel chips that could electrically detect surface-fixed DNA outside of the laboratory environment [22], [23]. The use of transistors as detectors bears advantages of simplicity, low cost, real-time detection, and relatively fewer detection equipment necessary; thereby, reducing the overall detection cost and allowing real-time detections regarding bio-detection. Preparation of bio-detectors via

7
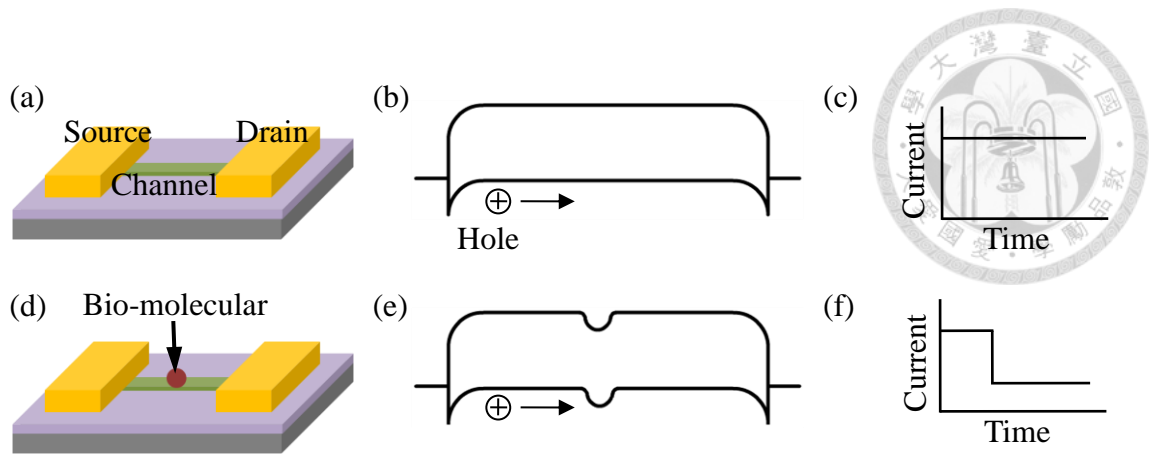
Figure 1-3 The detection mechanisms of bio-detectors [24].

the modification of transistors with antibodies is shown in Figure 1-3. Figure 1-3(a) and

Figure 1-3(b) show the component structures of bipolar transistors and the

band-structure diagram of typical p-type materials. Figure 1-3(c) depicts the source and

drain voltage measurements. When a polar molecule becomes attached to the transistor

channel, as represented by Figure 1-3(d), the band structure will change, as shown in

Figure 1-3(e), and the voltage will decrease for a p-type transistor (Figure 1-3(f)). The

voltage change translates to successful bio-detection.

1.2.2　Biosensor based on graphene

Current demands in bio-detectors include greater sensitivity, reduced

manufacturing cost, and shorter detection time. After Novoselov, K. S. and Geim, A. K.

discovered graphene by mechanical exfoliation in 2004, graphene's superior electrical

[25], mechanical [26], optical [27], and heat transfer properties [28] have been validated

8

by several laboratories. Owing to its characteristic electron transport potential, graphene's carrier transport is highly influenced by the surroundings and minor changes in the environment can affect the resistance or conductivity [29]. Moreover, surface modification of graphene is simple and biomolecules can be conjugated to graphene. Therefore, graphene-based bio-detectors are considered ideal detection platforms. Similar to most nanomaterials, a functionalization process is required for the covalent binding biomolecules with graphene. Furthermore, this method should prevent the formation of single-layer graphene defects in order to maintain device performance.

Mohanty and Berry were the first to study the application of graphene on bio-devices [30]. In their study, chemically modified graphene (CMG) was used to prepare bio-devices with single-bacterium resolution, DNA detection ability, and bacterial DNA/protein sensing capability. CMG demonstrates semiconductor properties and is extremely sensitive to the capture of molecules which results in changes in the carrier molecules. A typical preparation process utilizes the Hummers method [31] to modify the graphene oxide (GO) surface with epoxy, hydroxyl, and carboxylic acid groups. On the other hand, the test strip is plasma-treated to generate amines. The test strip is then submerged into the GO solution and a layer of 1-5 nm GO is deposited by electrostatic deposition, followed by the formation of covalent bonds between DNA's amine groups and GO's hydroxyl groups. In the meanwhile, areas of the test strip not

9

covered by GO have terminal amines that do not react with DNA. Thus, selective detection is achieved. By using similar methods, other teams have proposed bio-sensors based on the conjugation of graphene with aptamer [32], [33], [34], [35].
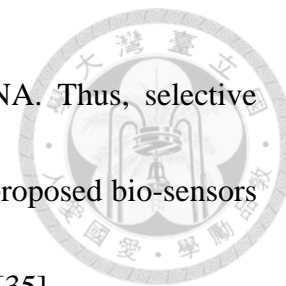
1.2.3　Reduced graphene oxide

In recent decades, laboratories have used the chemical vapor deposition (CVD) method to successfully produce large areas of graphene from the surface of transition metals, resulting in their extensive popularity and study [36], [37]. This method allows the production of large-area graphene and can be applied to other matrices as well [38]. One example is wet-transfer printing where graphene is shifted on to polymeric materials to provide support [39], [40]. Then, an etching solution is used to etch the metal film. This is followed by the transfer of the graphene and the polymeric material to a desired matrix. However, during the transfer process, defects may arise to help relieve the mechanical stress in the graphene's structure.

Graphene oxide (GO) is prepared by the dispersion of graphite bulk via chemical exfoliation, followed by the Hummer's method. Thus, GO is different from the graphene prepared via CVD. The matrix surface and the borders of GO contain high coverage of oxide functional groups. Figure 1-4 and Figure 1-5 depict the chemical structures of graphene and GO respectively.

10
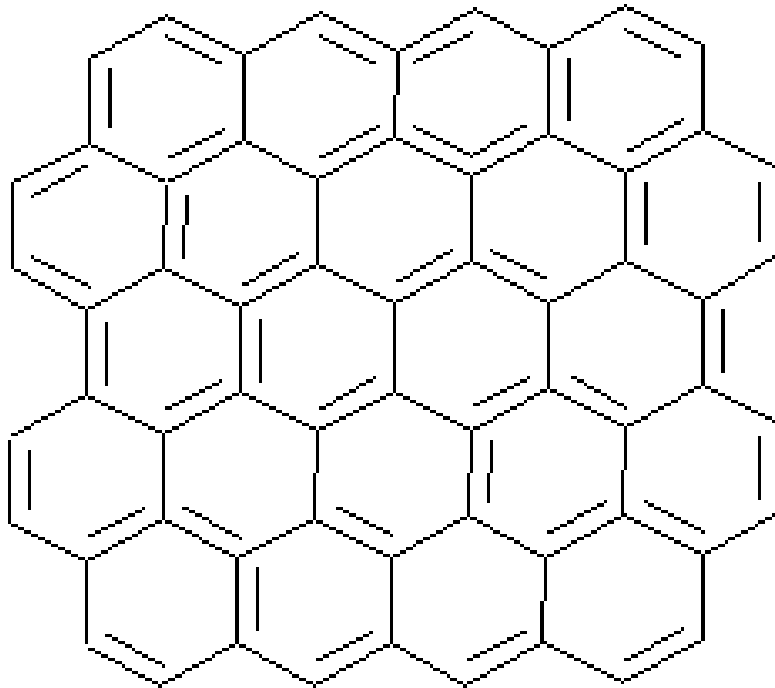
Figure 1-4 Chemical structure of graphene.
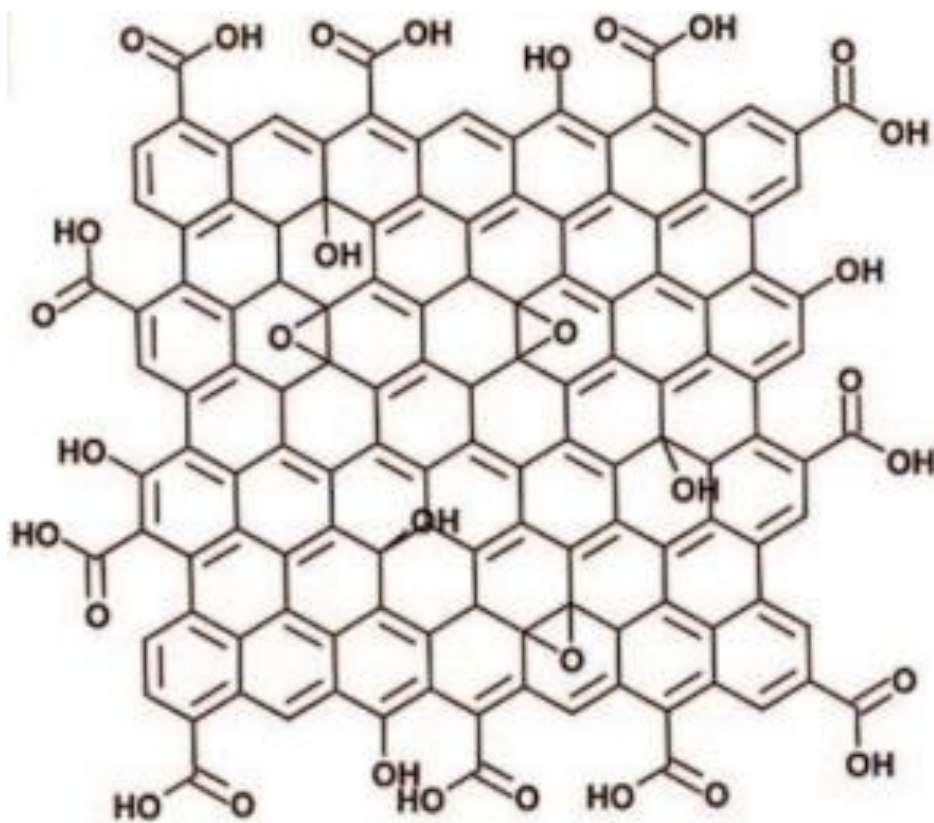
Figure 1-5 Chemical structure of graphene oxide.

11
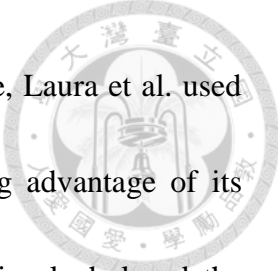
In comparison to graphene, GO is easier to prepare and lower in cost. In general, graphene materials have the advantages of mass production by solution processed fabrication and simple modification by subsequent chemical functionalization, among others which result in their potential for a wide spectrum of applications. This study prepared, through a reduction process, reduced graphene oxide for use as the sensor-region material in a bio-FET (field-effect-transistor). By the detection of a change in source and drain or a shift in the Dirac point, different concentrations of biological proteins can be measured. Furthermore, GO exhibits other characteristics including increased detection sensitivity, reduced detection time, elimination of large detection systems, and significant reduction of costs. Moreover, using different antibodies to modify the detection region allows the detection of corresponding antigen proteins. However, for product development, there are still manufacturing difficulties that remain to be resolved. For example, bio-chips must have identical height and their rapid mass production in large areas is also desired. Therefore, this study emphasized the control of graphene dispersity as well the material thickness.

1.3   Literature review

1.3.1   Langmuir-Blodgett method

Different from graphene prepared via CVD, the surface and borders of GO

materials exhibit high oxide group density. As described in literature, Laura et al. used

GO to prepare homogenously distributed graphene [41]. By taking advantage of its

ability to distribute homogenously in solution, GO was dispersed in alcohol and the

solution was added to the surface of purified water via the Langmuir-Blodgett method

[42],[43]. The dip-coating method was used to homogenously disperse GO on to the

matrix surface. Because graphene size affects dispersity, a centrifuge was used to extract

GOs within a desired size range so that materials do not overlap during the process;

thereby, realizing the ideal single-layer graphene oxide deposition on the matrix.

1.3.2 SAMs (Self-assembly) method

In 2013, Chang et al. developed a GO based bio-chip that was able to detect the

concentration of *E. coli*. The group used the sputtering method to deposit comb-shaped

Au electrodes on to wafers [44]. Briefly, GO was dispersed in purified water and

aminoethanethiol (AET) was used to functionalize the Au electrodes. Next, the

drop-casting method was used to disperse GO on to the prepared Au electrodes. By

exploiting the self-assembly property of GO and AET, GO was bridged between the Au

13
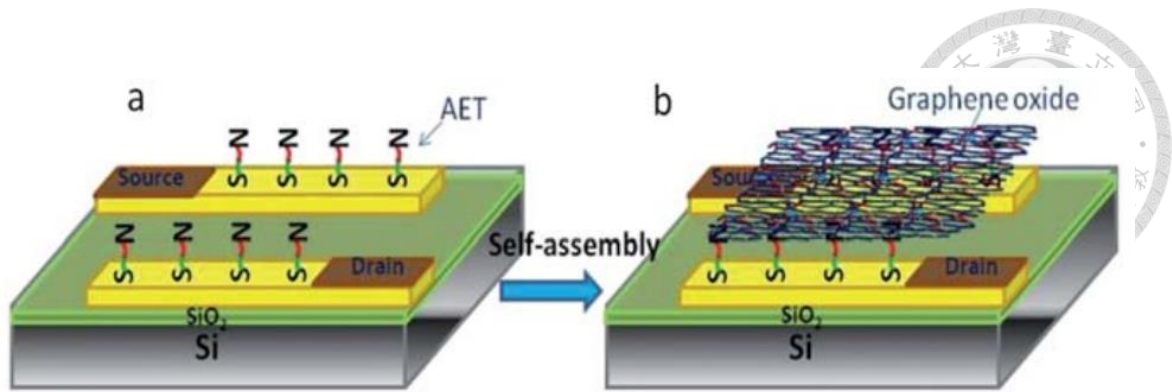
Figure 1-6 Self-assembly of GO sheets on the AET-modified electrodes [44].

comb-like electrodes. Figure 1-6 depicts the SAM method. Next, thermal annealing was

used to reduce GO to graphene. Because the oxide functional groups on the original GO

were partly reduced, the reduced GO also bears graphene properties. Next, the antibody

for *E. coli* was covalent grafted on to the graphene and non-grafted moieties were

blocked with Tween 20. Results revealed that when the *E. coli* concentration increased,

the voltage change detected also increased.

1.3.3   Spin-coating method

In 2013, Bykkan et al. studied the preparation of graphene oxide thin films via spin

–coating [45]. In this study, graphene oxide aqueous suspension with a concentration of

0.05g of GO was suspended in 20ml water of and 20ml of ethylene glycol in two

different beakers. 2g of PVP (Polyvinyl Pyrrolidone) was added to the aqueous solution

for increasing viscosity. The GO suspension was then spin coated at 2000-7000 rpm for

30s with spin coating equipment on FTO (fluorine doped tin oxide), ITO (indium tin

14

oxide) substrates and glass slides. After spinning, the GO thin films were dried at room

temperature for 24 hrs.

The thickness of the thin film was measured by Profilometer. The average

thickness of ethylene glycol used thin film was obtained as 73.6nm, 37.4nm, 22.3nm,

20.5nm, 15.5nm and 13nm at 2000, 3000, 4000, 5000, 6000 and 7000 rpm respectively.

The average thickness of water used thin film was obtained as 346 nm, 98.6 nm, 56.3

nm, 45 nm, 31.6 nm, 19.8nm at 2000, 3000,4000, 5000, 6000 and 7000 rpm

respectively.

In this paper, authors have fruitfully made GO thin films by using different

substrates with the help of spin coater and observed an inverse relation between the

thickness of the thin film and the rpm used at spin coating.

1.4   Motivation

The reduced GO was used as sensing material for bio-detectors for an effective and

probable strategy. However, for product development, there are still manufacturing

issues that must be addressed. Issues that must be resolved before commercialization

include the control of bio-chip height as well as the mass production of large material

areas. Therefore, this study proposed and discussed a method for distributing GO thin

film uniformly on to the bio-detectors. Herein, the spin-coating method was employed

because it is a highly efficient and rapid preparation method commonly used in the manufacturing of microelectromechanical systems. It is also a standard processing method for the manufacturing of integrated circuits and thin film liquid crystal displays [46]. The rotation of the substrate at high speed produces a centripetal force which pulls the coating solution into a nano-scale uniform thin film. Additionally, both the parameters and quality of the GO thin film can be finely tuned by the spin-coating. Thus, by using a solution of dispersed GO, the spin-coating method can be employed to produce relatively GO thin films.

Chapter 2   Spin Coating Theory

2.1   Introduction to spin-coating

Spin coating is a cheap and fast method to produce a homogeneous layer. This method was first described by Emslie et al. (1958) [46] and Meyerhofer et al. (1978) [48] using several simplified apparatus. Excess amount of solvent is placed on the substrate, which is then rotated at high speed for spreading the solvent by centrifugal force. The film thickness can be adjusted by changing the spin rate, the rotation time, and the viscosity of the solution. The disadvantage of this method is that it is limited by the solvent and its lack of material efficiency. Thin films produced by spin-coating are highly uniformity and can be simple controlled by the production parameters. Thus, this method can be used for the low-cost mass production of large-area chips. This is the rationale for the selection of this method in this study.

Centripetal acceleration will cause most of the resin to spread to, and eventually off, the edge of the substrate, leaving a thin film of material on the surface [49]. In this process, excessive amount of suspension is placed on the substrate and then rotated at a high speed in order to spread the fluid by centrifugal force. Resulting from the centripetal acceleration, most of the suspension is flung off the edge of the substrate, leaving a thin film layer. After the evaporation of the dispersions, a thin film of particles was formed on the wafer surface.
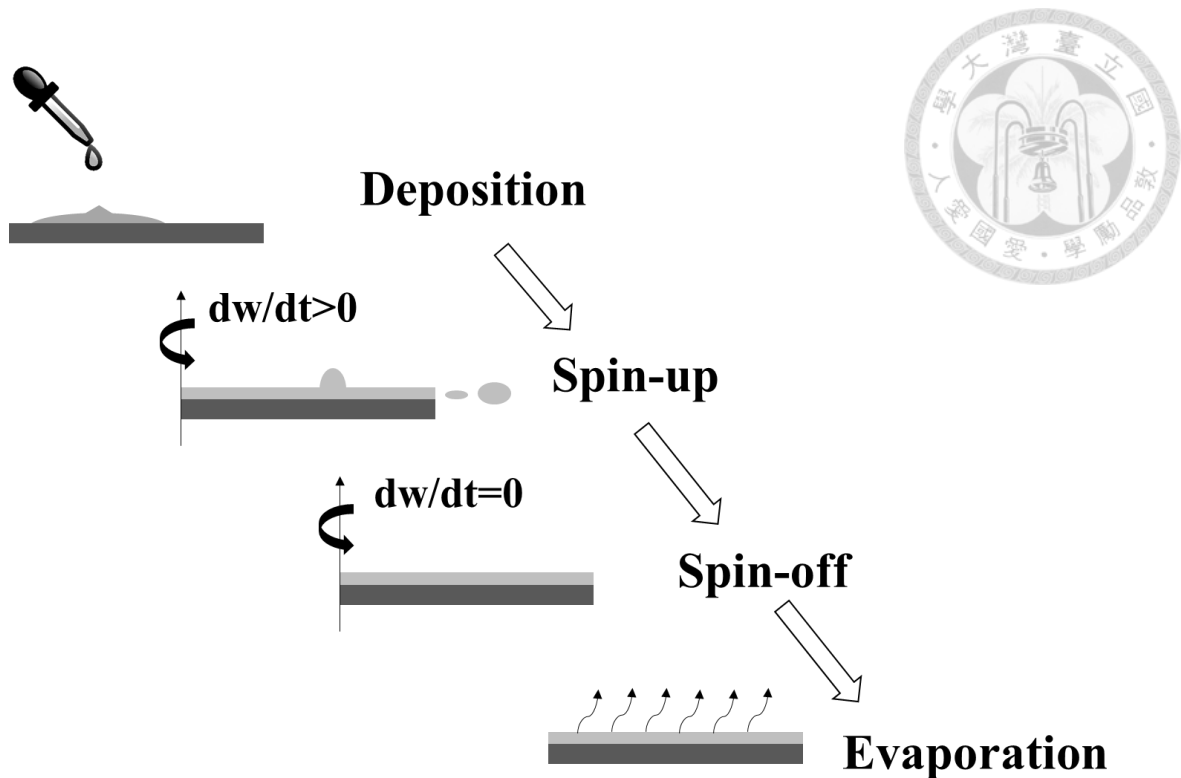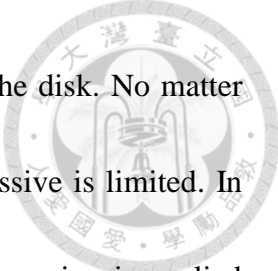
Figure 2-1 Key stages of spin coating process.

The whole spin-coating process is shown in Fig 2-1. The process can be divided into four distinct stages for modeling the physics of the process [50]. The four stages are deposition, spin-up, spin-off and evaporation of solvent, respectively. From the Fig 2-1, the last two stages were overlapped. These last two stages have great impact on final produced film thickness. The four stages are described in detail in the following:

Deposition stage:

In this stage, dispersions can be deposited in different ways: (a) as a large drops that inundated the entire substrate; (b) as a bubble at the center, the dispersions then spread over the rest of the disk; (c) as a continuous stream at the center, or the combined

these ways around the inner, then the liquid flowing outward over the disk. No matter

what way is used the amount of dispersions deposited through excessive is limited. In

this research, the way (a) was employed. An excess amount of suspension is applied

onto the center of the substrate by a micropipette.

Spin-up stage:

In the second stage, the substrate is accelerated up to a relatively lower speed.

Large amount of the dispersions is ejected from the substrate surface due to the strong

rotational motion. During this stage, the spiral vortices may briefly be present because

of the initial height of fluid on the substrate center surface. The spiral vortices will make

the twisting motion due to the top fluid layer inertia exerts when the substrate rotates

faster and faster. Then the substrate is accelerated up to a higher rotation speed. Finally,

the substrate reaches its desired rotation speed and the fluid become thin resulting from

the viscous shear drag exactly balances the rotation accelerations.

Spin-off stage:

At the third stage, the substrate is spinning at a constant rate and fluid is stably out

flowing.   The viscous force dominates the gradual fluid thinning behavior in this stage.

Even the solutions containing volatile solvents, the fluid thinning is generally quite

uniform.   The thickness equation of the spin-coating method was described in this

stage mainly.

Evaporation stage:

When the spin-off stage ends, the film begins to evaporate the solvent. In this stage substrate still spins at a constant rate, but centrifugal outflow stop and solvent evaporation caused the film further thinning. With the loss of solvent, the suspended or dissolved solids become highly concentrated and form a high viscosity, low diffusivity layer or a solid film. Coated film is quite uniform in the central area of the substrate but not so perfect at the edges. This is because the fluid flow outwards and forms droplets at the edges which became thicker film at the end [51].

2.2   Spin coating thickness equation

Graphene is an allotrope of carbon in the form of a two-dimensional honeycomb lattice. Its sensitivity as sensor material is increased when the structure approaches single-layer. The GO used in this study generally retains its original hexagonal lattice. However, on the basal plane and edges, large numbers of oxygen functional groups are present [52]. Therefore, the adequate control of the thickness of the deposition of GO on to the sensor is critical importance. Herein, the method of controlling film thickness by the spin coating method will be discussed.
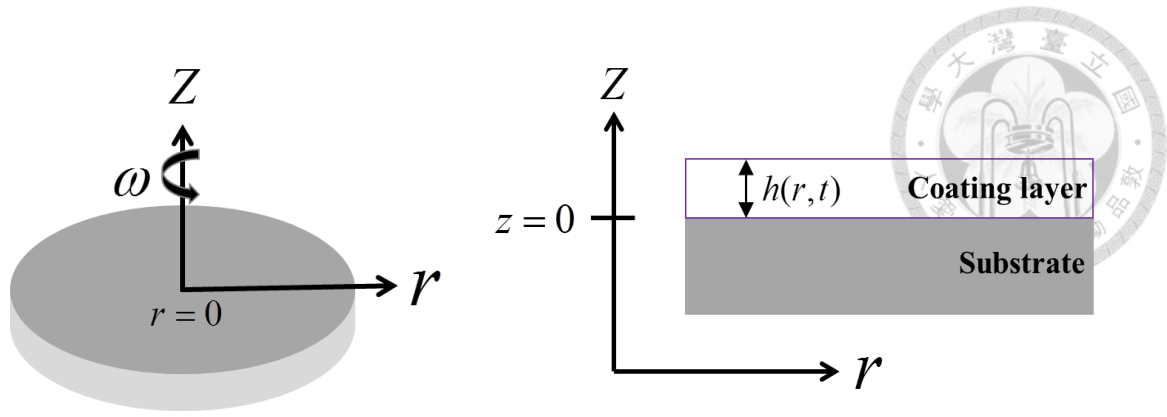
Figure 2-2 Spin-coating model schematic.

Final film thickness and other properties depend on the features of the solution and the parameters of the spin-coating process. The features of the solution are viscosity, drying rate, concentration of the solid, and surface tension. The factors of the spin-coating process are amount of the delivered solution, final spin rate, acceleration, and spin time [52].

Herein, Washo's theoretical model was adopted [55]. Using cylindrical polar coordinates (r, θ, z) with origin at the center of rotation, where z axis is perpendicular to the plane and the axes r and θ rotate with the plane with angular velocity ω. This model schematic is shown in Fig 2-2. The balance between viscous and centrifugal forces per unit volume for Newtonian fluid is given by

$$-\eta(\frac{d^2v}{dz^2}) = \rho\omega_f^2 r \tag{2.1}$$

where η is absolute viscosity, ρ is fluid density, v is velocity in the direction of r, ω_f is the final spin rate. Integrating with respective z and using boundary condition of zero

21

shears at the free surface.

B.C.

$$\partial v / \partial z = 0$$
$$at \ z = h$$

(2.2)

and

$$v = 0$$
$$at \ z = 0$$

(2.3)

Solution of the equation:

$$v = \frac{1}{\eta}(-\frac{1}{2}\rho\omega^2 rz^2 + \rho\omega^2 rhz)$$

(2.4)

The radial flow per unit length of the circumference q is given by:

$$q = \int_0^h v(z)dz = (\rho\omega^2 rh^2)/3\eta$$

(2.5)

The equation for continuity is given by:

$$r(\frac{\partial h}{\partial t}) = -\frac{\partial(rq)}{\partial r}$$

(2.6)

Applying eq. (2.5) in eq. (2.6) yields:

$$\frac{\partial h}{\partial t} = -K(\frac{1}{r})\frac{\partial(r^2 h^3)}{\partial r}$$

(2.7)

where $K = \rho\omega^2/3\eta$

Considering the special solution, which it depends only on the time t.

Special solution:

$$\frac{\partial h}{\partial t} = -2Kh^3 + 3Krh^2\frac{\partial h}{\partial r}$$

(2.8)

Because the film is uniform in the beginning, h is independent of r and hence

$\partial h / \partial r = 0$ which gives:

22

$$\frac{dh}{dt} = -2Kh^3 \qquad\qquad (2.9)$$

Integrating both sides between proper limits I.C. at $t = 0$, $h = h_0$ and at t , $h = h_t$,

equation (2.8) become as:

$$h_t = h_0 / [1 + 4h_0^2 \rho \omega^2 t / 3\eta]^{1/2} \qquad\qquad (2.10)$$

where h_t is final film thickness and h_o is the end of spin-up stage thickness.

This result does not take into account the effects of the fluid rheology and

evaporation. The evaporation rate will be calculated and estimated by the experiment

results. The mathematical modeling of the process is quite challenging. A simple

model has been established by Meyerhofer, who has presented a model for the spin

coating process which takes into account the evaporation of the solvent.

According to Meyerhofer module [56], the final film thickness of a spin-coated

layer depends on the process and material parameters, such like spin rate, viscosity and

solvent evaporation rate by the semi-empirical formula as shown in eq. (2.11).

$$h_t = \left(1 - \frac{\rho}{\rho_0}\right) \bullet \left(\frac{3\eta\phi}{2\rho_0\omega^2}\right)^{\frac{1}{3}} \qquad\qquad (2.11)$$

where h_t is final thickness, ρ is the density of the solvent, ρ_o is the initial value of ρ,

and ϕ is the evaporation rate of the solvent. Meyerhofer has found that the film

thickness h_t shows the following dependence on spin rate ω, initial viscosity η, and

evaporation rate ϕ. Assuming there is no evaporation loss of solvent, the relationship

23
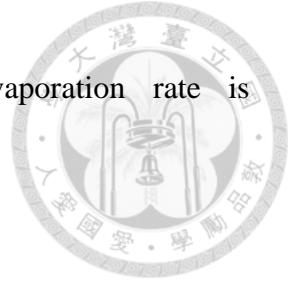
between film thickness, spin rate, initial viscosity, and evaporation rate is

$$h_t \propto \omega^{-2/3} \eta^{1/3} \phi^{1/3} \quad .$$

2.3   Spin coating rate & GO film thickness

In most applications, the parameters: viscosity, evaporation rate and solvent density, change during the coating process.   Therefore, the using of spin rate to control thickness is a more appropriate strategy.   According to Washo's theoretical model, the relationship between the film thickness, the spin rate and the time is:

$$h_t \propto \omega^{-1} t^{-1/2} \tag{2.12}$$

However, Washo's theoretical model assumes that (a)the spinning fluid is Newtonian, (b)constant volumetric fluid flow on and off the disk, (c)no evaporation loss of solvent (therefore η is constant), and (d)no body or surface force, that do not agree with the actual situation.   On the other hand, according to the Meyerhofer model, the relationship between the film thickness and the spin rate is:

$$h_t \propto \omega^{-2/3} \tag{2.13}$$

However, Meyerhofer also assumes that there is no evaporation loss of solvent.   If the evaporation rate varies with the square root of the spin rate, then the relationship between the film thickness and the spin rate is modified as [56]:

$$h_t \propto \omega^{-1/2} \tag{2.14}$$

24

This formula only can guide the experiments, but the parameters related to the film thickness are determined empirically in practice. According this, a more simple formula always used is:

$$h_t = A \cdot \omega^{-B} \qquad (2.15)$$

where *A* and *B* are constant parameters that should be calculated experimentally. In most cases, *B* was determined to be in the interval between 0.5 and 1 [57], which is in considerably agreement with eq. (2.13) and eq. (2.14), where the exponent for ω is 0.67 and 0.5 , respectively.

The present theoretical models were all established for organic solutions not for colloidal particle or sheets dispersions. The eq. (2.13) and eq. (2.14) are used for estimating the continuous thickness of the organic solution films. These equations are not appropriate for particle films due to the particle film thickness are discreet and decided by the particle diameter. Therefore, these equations above are used as suitable reference for estimating the experimental parameters.

The range of spin rate is a key point because it defines the range of the thickness that can be implemented by given solution. Generally, we can produce uniform films easily from about 1000 rpm upwards. Most common spin coating will also reach maximum speed of 6000-8000 rpm. As such, range of rotation speed might is the important thing that we should note [45].

25

2.4 Spin coating with solvent blends

The evaporation rate of the solvent also plays a critical role in the process of spin-coating. If a low boiling point, i.e. high evaporation rate, solvent is used, the coating process can be achieved easily and an amorphous film is produced. If a high boiling point, i.e. slow evaporation rate, solvent is used, the coating process is difficult to carry out because the ink needs time to evaporate and is flung off the edge of the substrate.

The mixing of two different solvents, one with fast evaporation rate and one with slow evaporation rate, is an excellent method for increasing spin uniformity [57]. Figure 2-3 shows the spin coating processes with different evaporation rate solvent blends. During spin coating process, the higher evaporating solvent will quickly evaporate to promote thin film coverage and uniformity. The slower evaporating solvent remains and provides sufficient time for the rearrangement of the solute. Mixture of high evaporation rate solvent and slow evaporation rate solvent was employed for thereby allowing complete arrangement and promoting uniformity.
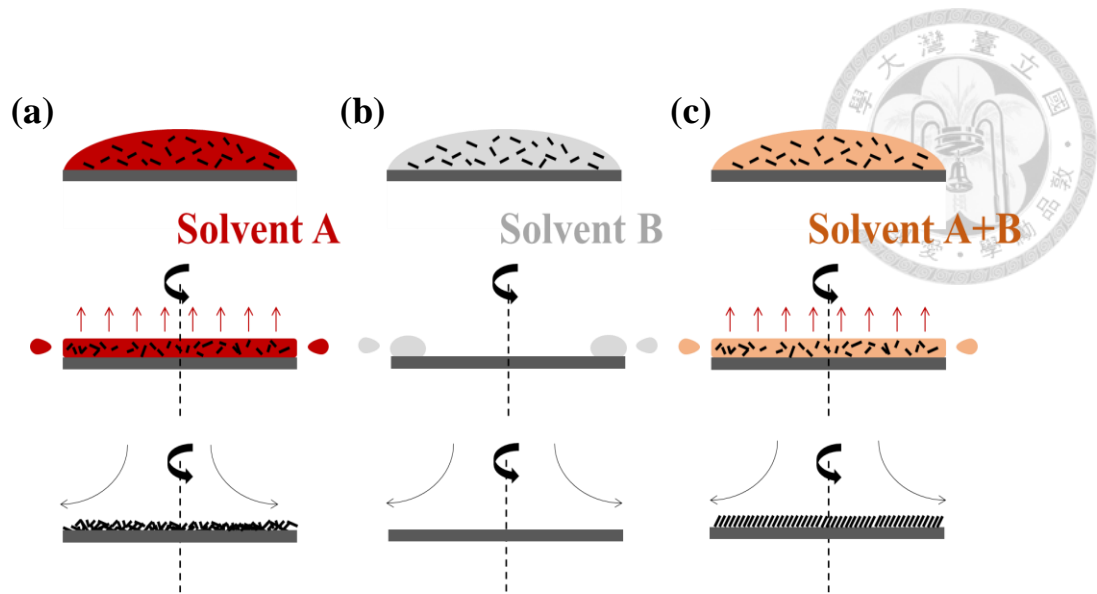
Figure 2-3 Spin coating with solvent blends. (a) High evaporation rate solvent. (b) Slow evaporation rate solvent. (c) Mixture of high evaporation rate solvent and slow evaporation rate solvent.

Chapter 3   Fabrication

3.1   Materials

3.1.1   Substrate

In order to characterize the target for recognition of critical concentration using cTnI aptamer-functionalized biosensor, a batch of graphene-based field effect transistors were fabricated.   The substrate is p-type silicon wafer (5-10 Ω) as back gate and the dielectric layer was silicon oxide thin film grown from silicon at 280 nm in thickness. The reason for growing 280 nm silicon oxide is for the observation of graphene easily under optical microscopy after transferring the graphene onto silicon oxide surface.

3.1.2   Solution

GO dispersion on metal surfaces such as Au, Ag, Cu, and Al is difficult to be realized because of the lack of electrostatic interactions[57].   Besides, the contact angle of GO solution on these metal surfaces is large (in our experiment, contact angle > 80°) and difficult for depositing GOs.   As a result, the successful sample of GOs depositing on the metal surface is very limited.   It is known that the wettability between the solution and the substrate is affected by the properties of the solvent and the substrate. As described in section 2.4, the mixing of two solvents with different evaporation rates can be employed to improve the coverage and uniformity of the film.   The wettability

between GO solution and the metal surfaces was modulated by using mixed solvent of

methanol and water [59].

3.1.3 Cysteamine

Cysteamine is a compound that can be used self-assembly method on the gold

electrode and has been frequently employed as bifunctional building blocks, where the

sulfur atoms of the molecules bind to the gold surface while the amino groups may be

exposed on the gold surface [59].   Therefore, this study employed the amino groups of

the cysteamine to increase the hydrophilicity of the gold surface for improving the

quality of spin coating.
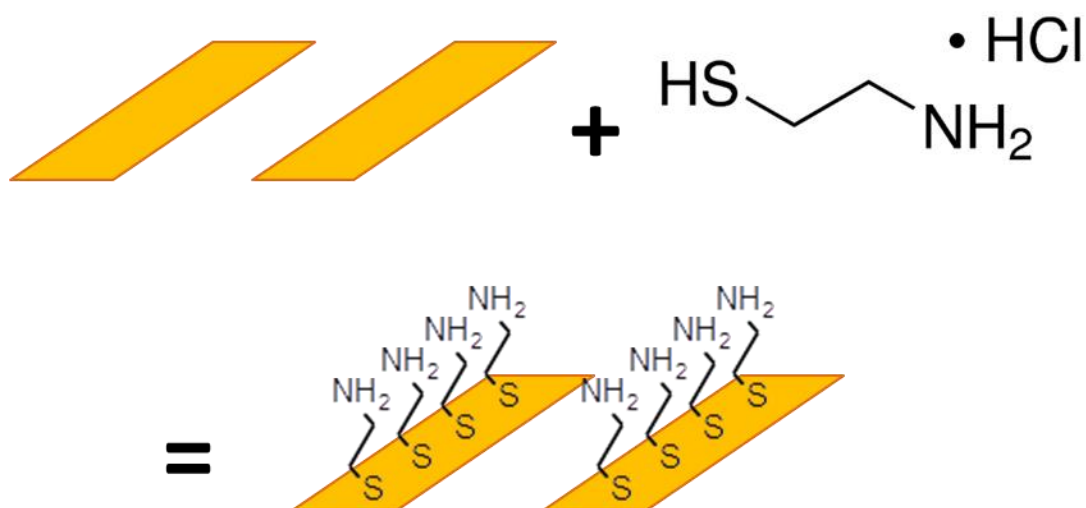
Figure 3-1 Cysteamine -modified electrodes by self-assembly method (SAM).

3.1.4 L-Ascorbic acid

L-Ascorbic acid (L-AA), having a mild reductive ability and nontoxic property, is naturally employed as a reducing agent in living things [60], and has also been used as a main reductant in the laboratory. Herein, a fluent approach for reducing GO sheets was presented by using L-AA as a reductant in an aqueous solution. More importantly, in comparison with the conventional reductants used in GO reduction, such as hydrazine and hydrazine hydrate, L-AA and the oxidized products are environmentally friendly [61].

3.1.5 Aptamer

Aptamer is a kind of the short and single stranded RNA (ssRNA) or DNA (ssDNA). It processes good plasticity in structure and strong affinity to specific targets such as amino acid molecules, viruses, proteins, and cells. There are more and more bio-sensors using aptamer as the sensing probe in recent studies [62-65] because the antibody has to be generated by immune system *in vivo* for long time and with high cost. Besides, aptamer can be selected *in vitro* by systematic enrichment of ligands by exponential amplification (SELEX) which has been successfully developed in the early 1990 [66-68]. The size of aptamer is much smaller than antibody, and the chemical properties of aptamer can be modified easily at designated for higher stability, stronger

bonding on substrate, higher sensitivity, and longer shelf life [69, 70].

3.1.6 Bio-molecules used in the experiment

1. The bio-linker between cTnI aptamer and graphene is 1-Pyrenebutyric acid N-hydroxysuccinimide ester. The bio-linker can be attached onto surface of r-GO via strong interaction between carbon lattice and pyrenyl group with π-π stacking in basal plane. The formula of 1-Pyrenebutyric acid N-hydroxysuccinimide ester is $C_{24}H_{19}NO_4$ and the molecular weight is 385.41 g/mol.

2. The cTnI aptamers were employed for binding to the bio-linkers during NHS ester reaction. The cTnI biomarkers can be captured specifically by cTnI aptamers. The sequence of cTnI aptamers used in this experiment is 5'-TCA CAC CCT CCC TCC CAC ATA CCG CAT ACA CTT TCT GATT-3'. The molecular weight is 11966.7 g/mol. And the primer length is 40 unit (U).

3. The ethanolamine (Sigma-Aldrich Inc.) is used to deactivate and to block the remaining NHS ester groups. The formula of ethanolamine is $C_{24}H_{19}NO_4$ and the molecular weight is 61.08 g/mol.

4. Cardiac troponin-I biomarker (Sigma-Aldrich Inc.) has been proved as the standard and an attractive biomarker for presymptomatic diagnosis. It is the main detecting

31

target in this research. cTnI biomarkers will bind with specific antibodies or aptamer.
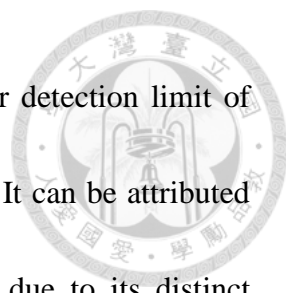
3.2 Device fabrication

The development of bio-chips can effectively lower the cost, detection time, and required specimen volume of blood examinations. In addition, the graphene bio-sensor chip used in this study is a field effect transistor. In order to realize the transfer of bio-chips from the laboratory to the public market, we adopted 150 mm silicon wafers with mass production as our target. The spin coating process is relatively fast and can be used to coat graphene uniformly onto 150 mm silicon wafers. Thus, this process was adopted in this study. For the silicon wafer, highly p-doped silicon wafer was used. The electron hole functions as a charge carrier in p-doped silicon wafers and thus its use as a matrix can allow current to pass and serve as the back-gate of the field-effect transistor. Firstly, the chip specifications were designed.

3.2.1 Design

For the chip design, a comb-shape structure was adopted for the electrode. The parallel electrode configuration has been extensively used for electrochemistry analysis. For example, in 2004, Yang et al. [71], [72] affixed biological antibodies to comb-shaped electrode prepared from indium tin oxide (ITO) for *E. coli* detection.

Results revealed that the impedance-based bio-detector has a lower detection limit of 10^6CFU/ml with linearity from 4.36 x 10^5 to 4.36 x 10^8 CFU/ml. It can be attributed to several advantages of parallel comb-shaped electrodes. First, due to its distinct geometry which is different from traditional electrodes, comb-shaped electrodes have greater detection area compared to traditional electrodes and can be arranged to provide greater sensitivity under limited space. Second, signal detection is adopted as the detection mechanism and does not involve the use of radioactive material, fluorescent reagent, biochemical enzyme, or chemical labeling
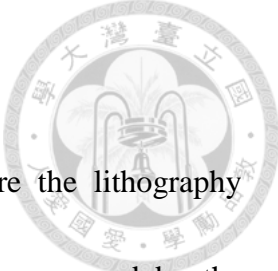
In this study, the detection region was designed to be comb-shaped in order to shorten the distance between source and drain, i.e. the channel length, to increase the detection sensitivity and increase the detection area of the detection region. The comb-shape electrode was designed with inter-distance of 2 µm and detection area of 400µm×500µm.   The bio-chip length and width are 3.5 mm, respectively.   Figure 3-2 shows the design of the detection chip.

(a)

3.5 mm

Sensor area

3.5 mm

(b)

2 μm
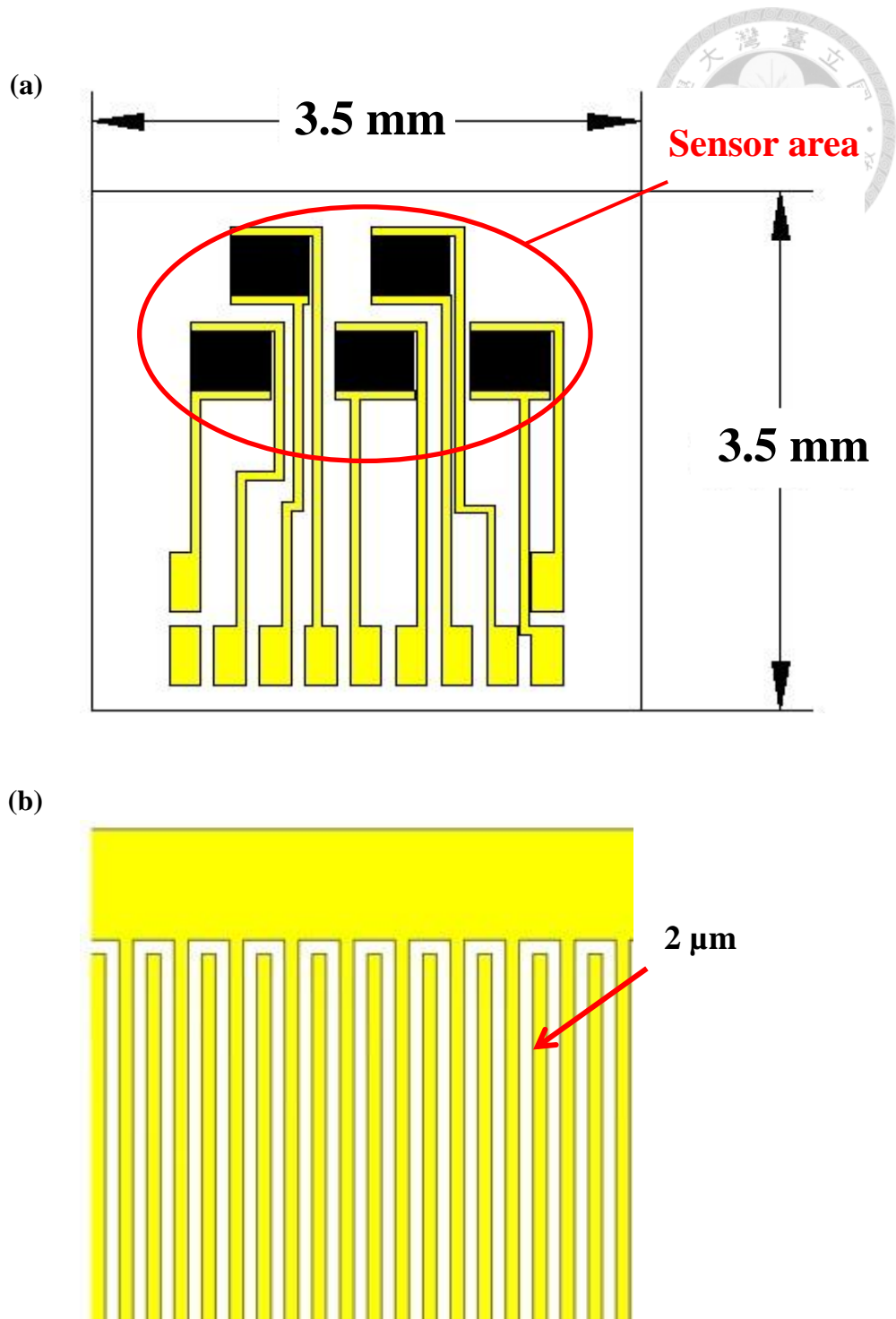
Figure 3-2 Design of the graphene detection chip: (a) Exterior appearance of the detection chip. (b) Comb-shaped electrode in the detection region.

3.2.2 Lithography
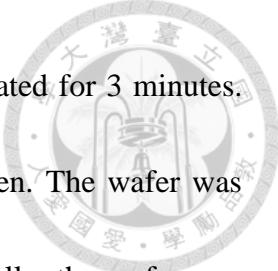
Patterns on the electrode were printed by lithography. Before the lithography process, inorganic contaminants on the silicon wafer surface were removed by the piranha solution (H_2SO_4: H_2O=3:1). The wafer was then cleaned with deionized water, and dried by a nitrogen gun. Next, the positive photoresist (SPR-220) was spin coated on the wafer as the mask layer. A photo mask was employed to pattern the desired section and a mask aligner was used to define the gate on the wafer for the exposure process. Then the silicon dioxide part of the gate was etched by reactive-ion etching (RIE) device to make a back-gate field effect transistor shown in Figure 3-3(a-b). After the previous photoresist was removed, the positive photoresist (SPR) was spin coated onto the wafer as a masking layer again shown in Figure 3-3(c). The photo mask in the shape of the desired comb-shaped electrode was used for the exposure pattern and processing to define the comb-shape shown in Figure 3-3(d). Then, a 10 nm titanium layer and 100 nm gold layer were evaporated by E-beam evaporation as the detection electrode shown in Figure 3-3(e). The titanium layer was used as the adhesion layer between the silicon oxide and gold electrode.
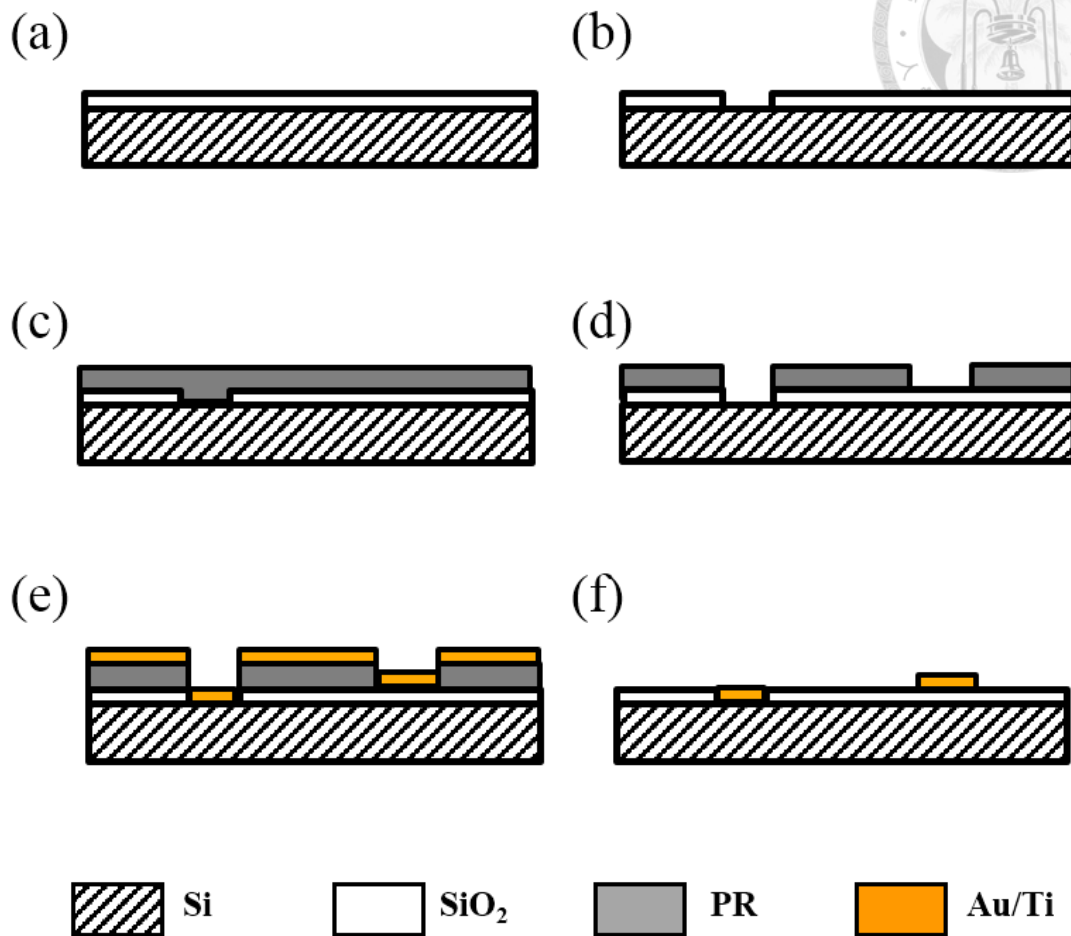
Figure 3-3 Schematic representation of the manufacturing process of the sensor wafer.

3.2.3 Lift-off methods

After evaporation process of the gold electrode was complete, acetone was used for lift-off process to obtain the final electrode shape shown in Figure 3-3(e-f). The evaporated wafer was immersed in 200 mL of acetone and sonicated at frequency of 40 K and power of 90 W for 3 minutes. Due to acetone is not miscible with D.I. water,

the wafer was transferred to 200 mL of isopropyl alcohol and sonicated for 3 minutes.

Then, the wafer was washed by D.I. water and dried by the nitrogen. The wafer was

then placed into D.I. water and sonicated for 3 minutes again. Finally, the wafer was

dried by the nitrogen to afford the comb-shaped electrode.

Because the inter-distance of the comb-shaped electrode is only 2 um, residual

gold fragments may cause short-circuit between the electrodes.   Thus, during the

lift-off process, the short-circuit-causing gold fragments was burnt-off by applying a

+10V bias voltage between the drain and source.   During the current applied, the

short-circuit-causing gold fragments were burnt-off by the Joule heating resulted from

the inherent resistance of the fragments.   Figure 3-4 shows the electrode before and

after passing a +10V bias voltage.

(a)

50 µm

(b)

50 µm
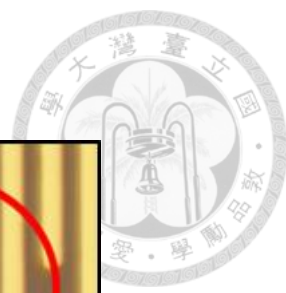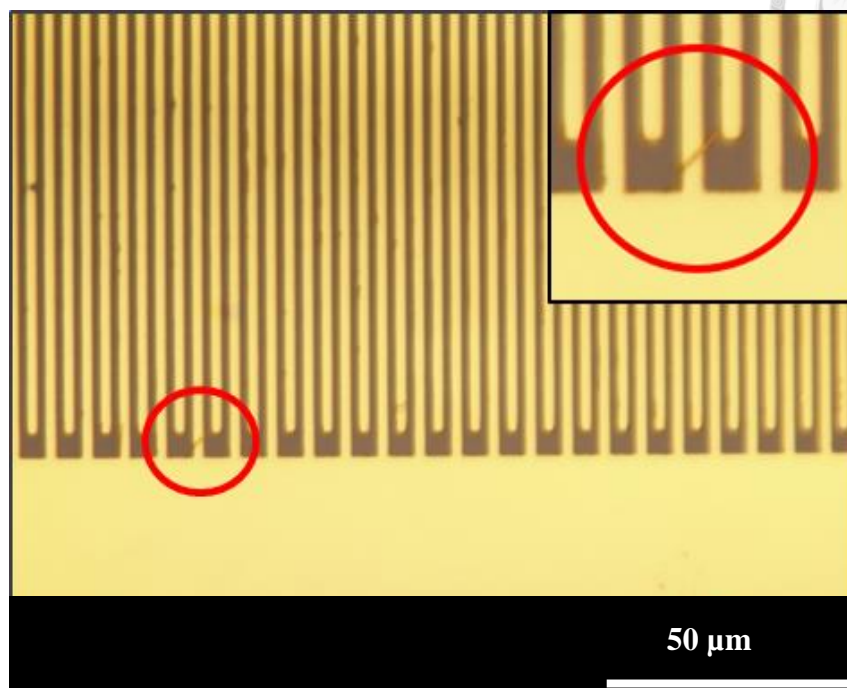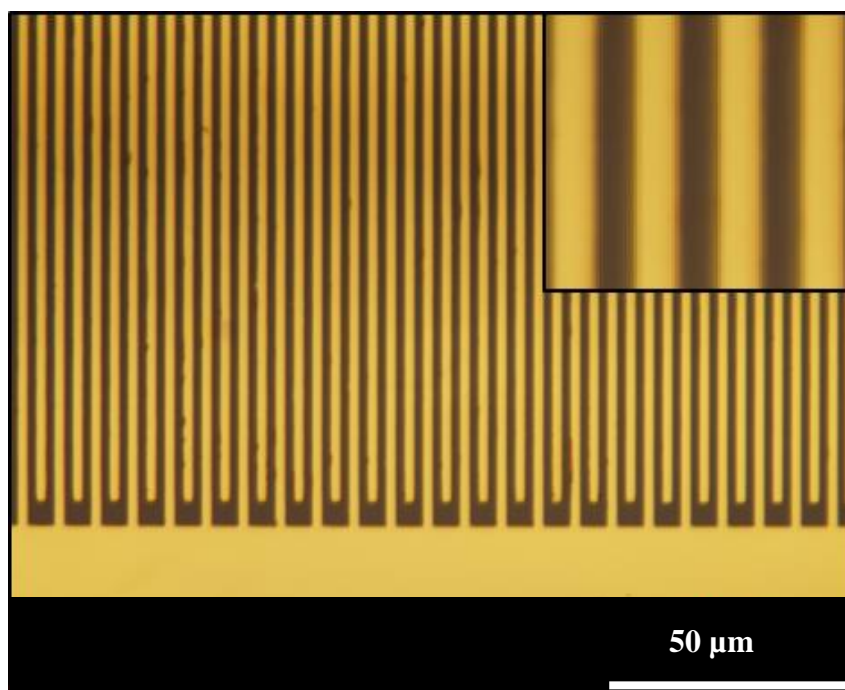
Figure 3-4 (a) Before applying a biased current. (b) After applying a biased current.

38

3.3   Experiment Prepare

In the spin-coating process, the solution wettability and the GO concentration determine the deposition position and GOs' coverage on the substrates.   The GO solution wettability is controlled by the test strip processing and solvent blends.   This section will describe the preparation process, including surface modification and solvent preparation.

3.3.1   Surface hydrophilization

In order to increase the hydrophilicity of the SiO_2 and gold surfaces, two different methods were used for their surface modification.   After the lithography process, the SiO_2 substrate was soaked in a piranha solution (H_2SO_4: H_2O=3:1) for 15 minutes to hydroxylate the surface and render it extremely hydrophilic. The involved chemical reaction was $H_2SO_4 + H_2O_2 \rightarrow H_3O^+ + HSO_4^- + O$.   Next, the substrate was washed with D.I. water and dried by the nitrogen.   After this process, the modification for the SiO_2 hydrophilic surface was done.   For gold surface modification, the gold electrode was immersed in a 30 mM cysteamine (3 mg/mL) solution for 12hr to allow a monolayer of cysteamine assembling onto the electrode.   Then, the gold electrode was washed with D.I. water and dried by the nitrogen. This concluded the hydrophilic surface modification of gold electrodes.
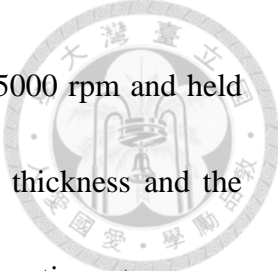
3.3.2 Graphene oxide dispersion

Different from graphene prepared by CVD, the surface and borders of GO materials exhibit high oxide group density. Due to the presence of these oxide groups, GO is a hydrophilic two-dimensional material that can be dispersed in aqueous solution. Firstly, the purchased GO was dispersed in D.I. water/methanol (1.5 mg/mL) and sonicated the solution for 2 hrs to disperse the GO in the D.I. water completely. Next, by referencing the result described in Sec. 2.4, two solvents with different evaporation rates were combined to increase coverage and uniformity. After sonication for 2 hrs, a homogenously dispersed GO/water/methanol solution was obtained.

3.4 Spin-coating process

Prior to spin coating, in order to increase the adhesion of the GO with the substrate, the chip was heated to 200ºC firstly. The chip was then placed in a pre-manufactured holder for spin coating. The spin coating process was divided into four phases as described in Sec. 2.1. First stage is the deposition, where 20 μL of mixture of GO/water/methanol was dropped onto the chip. In order to avoid the solution concentration change resulting from the evaporation, the next step was necessary to quickly proceed. During the spin-up stage, the spin coater was first operated at 500 rpm for 10 seconds in order to allow the solvent to form an initial film thickness. Then,

40

in the spin-off stage, the spin rate was gradually increased to 2000-5000 rpm and held

for 1-3 min.　This is the critical step that influenced the GO film thickness and the

thickness is directly related to the spin rate.　Finally, the evaporation stage was

conducted simultaneously with the spin-off stage.　After spin coating, the GO films

were dried at 90 °C on a hot plate.

3.5　Reduced process

After the GO film spin coating process, the next step involved the reduction of the

GO film.　Graphene oxide film on substrates were then reduced into graphene films by

L-Ascorbic acid solution (30 mg/mL) which was heated to 90 °C on the hot plate for 3

hrs.　After reduced process, the graphene films were washed with D.I. water and dried

by the nitrogen.

The preparation of the sensing region of the biosensor was completed after these

steps.　Finding a strategy of uniformly distributing graphene onto the biochip is an

important part in this section.　The next section involves the analysis and discussion of

graphene dispersion and uniformity.

3.6   Aptamer-functionalized process

After reduced process, the r-GO was functionalized with bio-molecules by sequential immersion in solutions. Firstly, the chip was immersed in 1-pyrenebutyric acid N-hydroxysuccinimide ester (NHS ester) of DMSO solution at 5 mM for 1 hour to attach the bio-linkers.   It was then rinsed with deionized water/DMSO and dried by N_2 gas.   Secondly, the chip was immersed in 10 nM solution of cTnI aptamers for 12 hours for attaching the cTnI aptamers.   The last step was to immerse the chip in 100 mM enthanolamine solution for 1 hour.   The graphene-based and aptamer-modified biosensor was entirely completed.
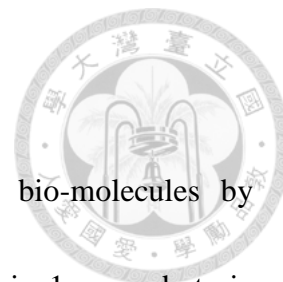
Chapter 4   Results and discussion

4.1   Contact angle analysis

4.1.1   Surface treatment

After soaking the SiO_2 substrate in the piranha solution, the surface of SiO_2 was hydroxylated.   Hydroxylation caused the SiO_2 surface become more hydrophilic so that the spin-coated GO may display better coverage and uniformity.   For gold electrode surface, the gold electrodes were soaked in cysteamine for collecting a thin layer of cysteamine on its surface as shown in Figure 4-1.   This SAM thin layer of cysteamine enhances the hydrophilicity of the gold electrode.

Contact angle analysis was conducted by a VCA OPTIMA instrument for estimating the surface treatment.   When 0.5 μL D.I. water was dropped to the sample surface, the VCA OPTIMA instrument captured the image of water contour and analyzed the contact angle by the software.   Figure 4-2 shows the images of a drop of water on SiO_2 and gold surfaces before the surface treatment.   For each surface treatment, twenty contact angle measurements were taken, averaged, and calculated for standard deviation.   Figure 4-3 shows the results of the surface contact angles of SiO_2 and Au electrode surfaces.

(a)
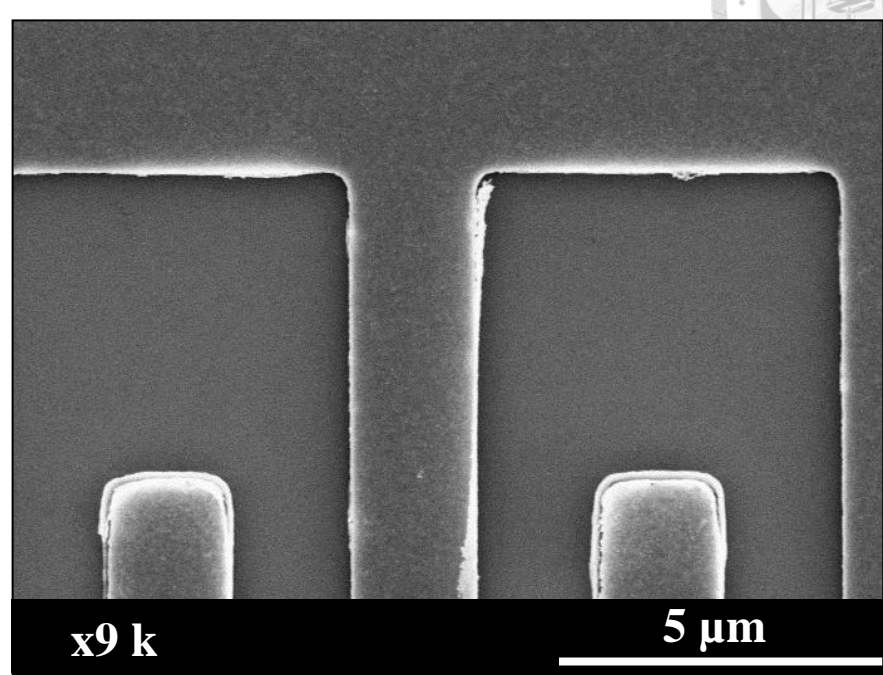
(b)
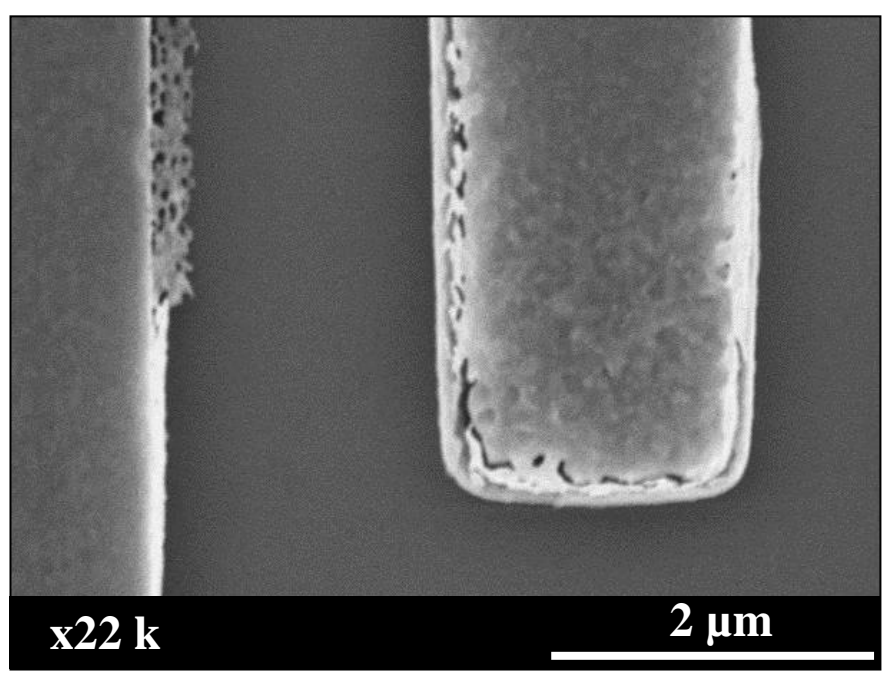
Figure 4-1 SEM image of cysteamine coating Au electrodes. (a) Image taken at a magnification of 9,000X. (b) Image taken at a magnification of 22,000X.

SiO₂ surface   **Au surface**
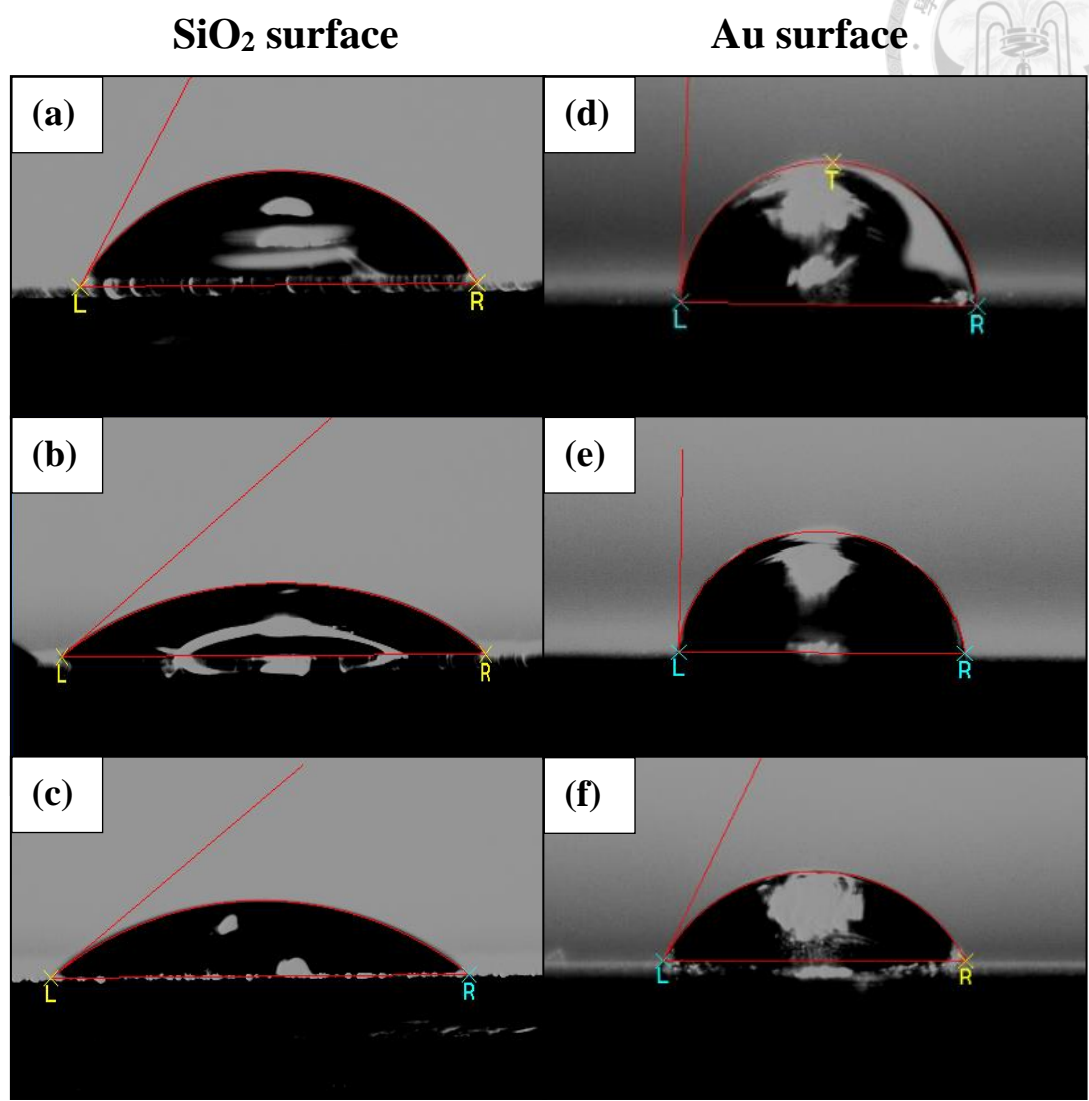
Figure 4-2 Contact angle images. (a) SiO$_2$ surface without treatment. (b) SiO$_2$ surface soaked with Piranha solution. (c) SiO$_2$ surface soaked with Piranha solution and cysteamine. (d) Au surface without treatment. (e) Au surface soaked with Piranha solution. (f) Au surface soaked with Piranha solution and cysteamine.

45
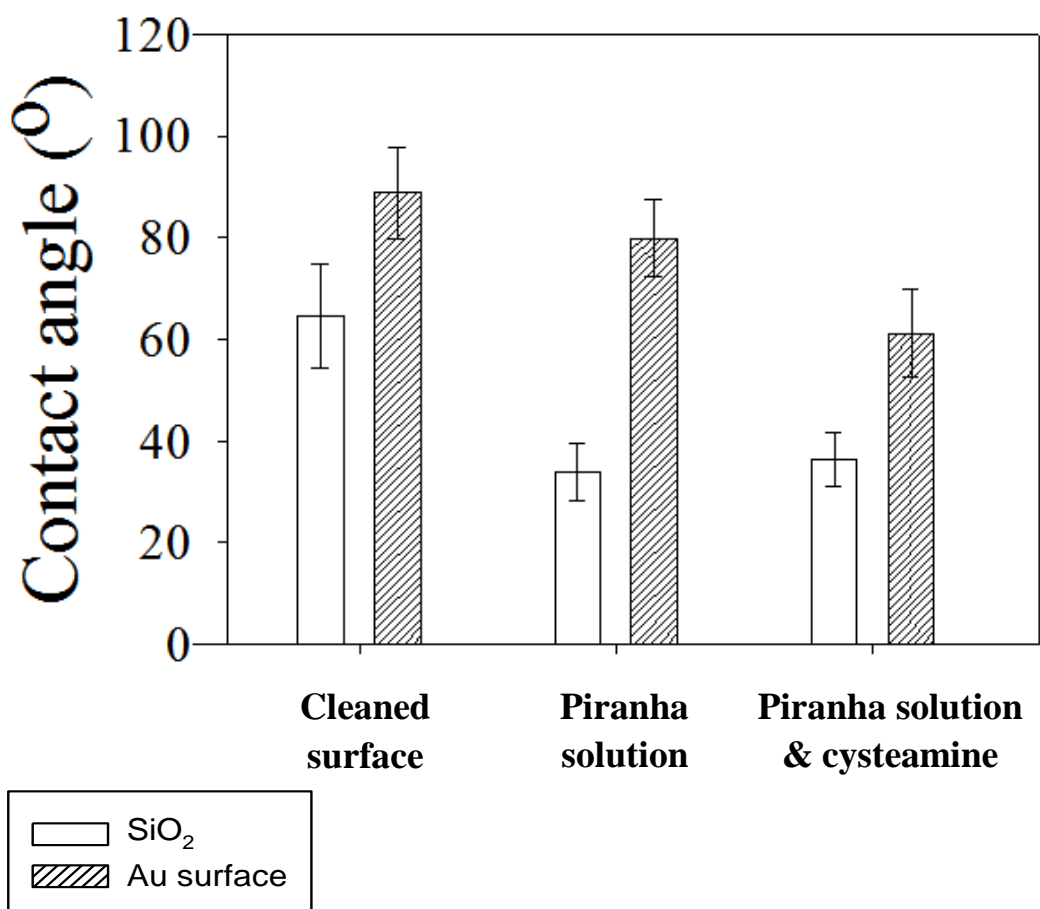
Figure 4-3 Contact angles of SiO$_2$ surface and Au electrode surface before and after modified by Piranha solution and cysteamine.

Result reveals that SiO$_2$ and Au electrode surfaces treated by piranha solution and cysteamine effectively enhanced the hydrophilicity. This is expected to promote GO coverage and uniformity in the following spin coating process.

4.1.2 Solvent blends

The use of a water/methanol mixture to disperse GO can enhance the hydrophilicity of the dispersant on the gold electrode surface. The relationship between contact angles of GOs on Au electrode surface and ratios of water/ethanol is shown in Figure 4-4 and Figure 4-5. Result reveals that the lower the water/methanol ratio has the greater the hydrophilicity on the gold electrode surface.
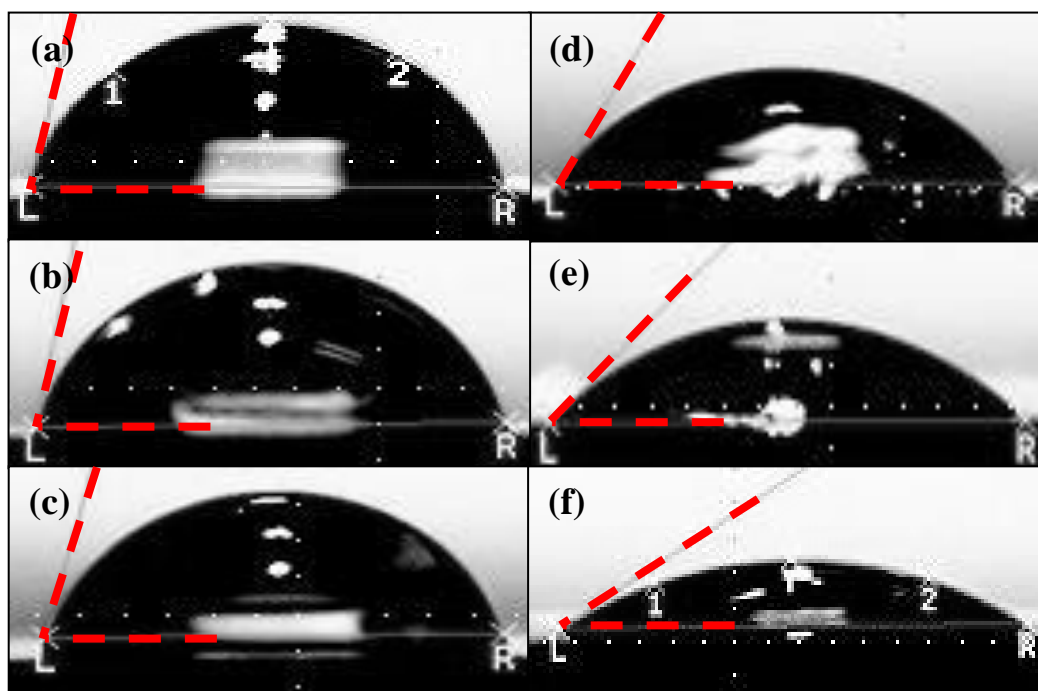
Figure 4-4 Contact angle analysis on Au surface with different water/ethanol ratios. (a) 10:1, (b) 5:1, (c) 2:1, (d) 1:1, (e) 1:2 and (f) 1:5.
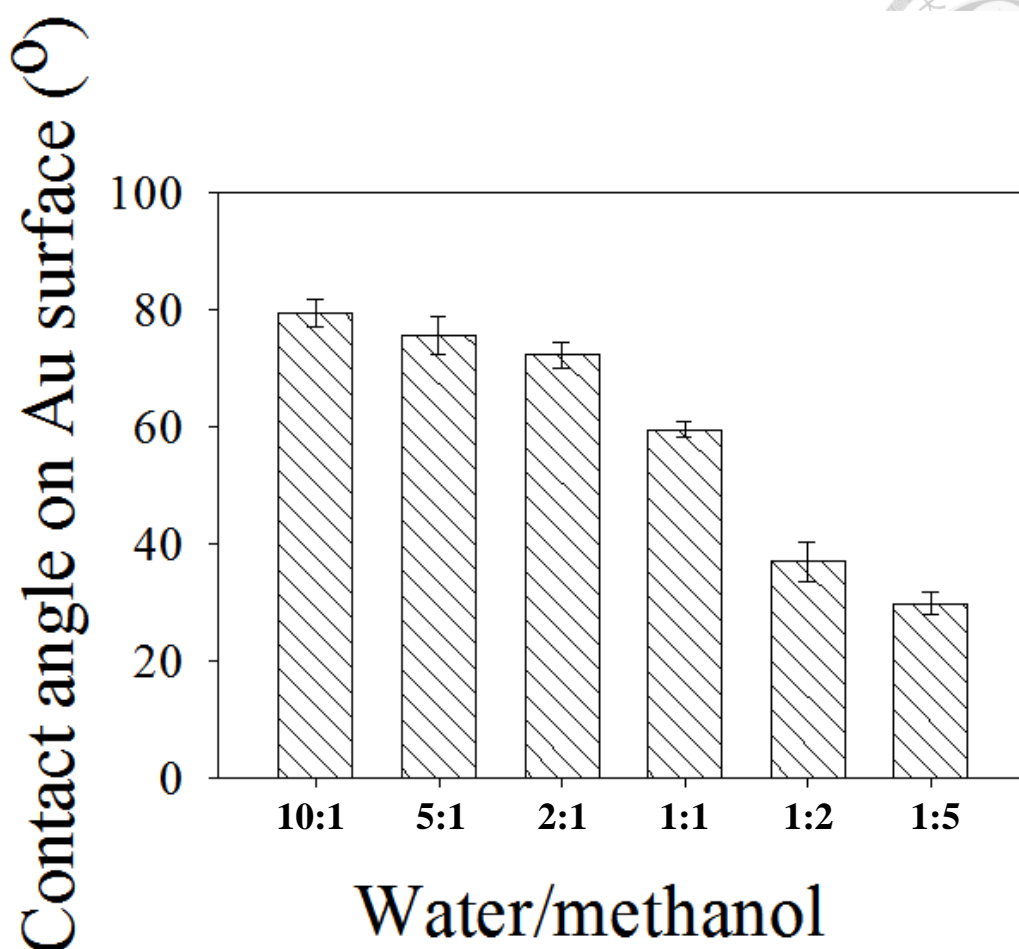
Figure 4-5 Contact angle analysis on Au electrode surface with different water/ethanol ratios.

The solutions of GO dispersed at different water/methanol ratio were spin coated on the Au electrode surface. For each sample, spin coating process was carried out and repeated for three times. The results are shown in Figures 4-6. From the results, when the water/methanol ratio was 10:1, 2:1, and 1:1, the GO thin layer demonstrated poor uniformity and significant aggregation. A water/methanol ratio of 1:2 is the most adequate formulation, and this ratio allowed the GO thin film to be uniformly

distributed on the chip.   After following reduction, the relationship between resistance

and the water/methanol ratio was obtained as shown in Figure 4-7.
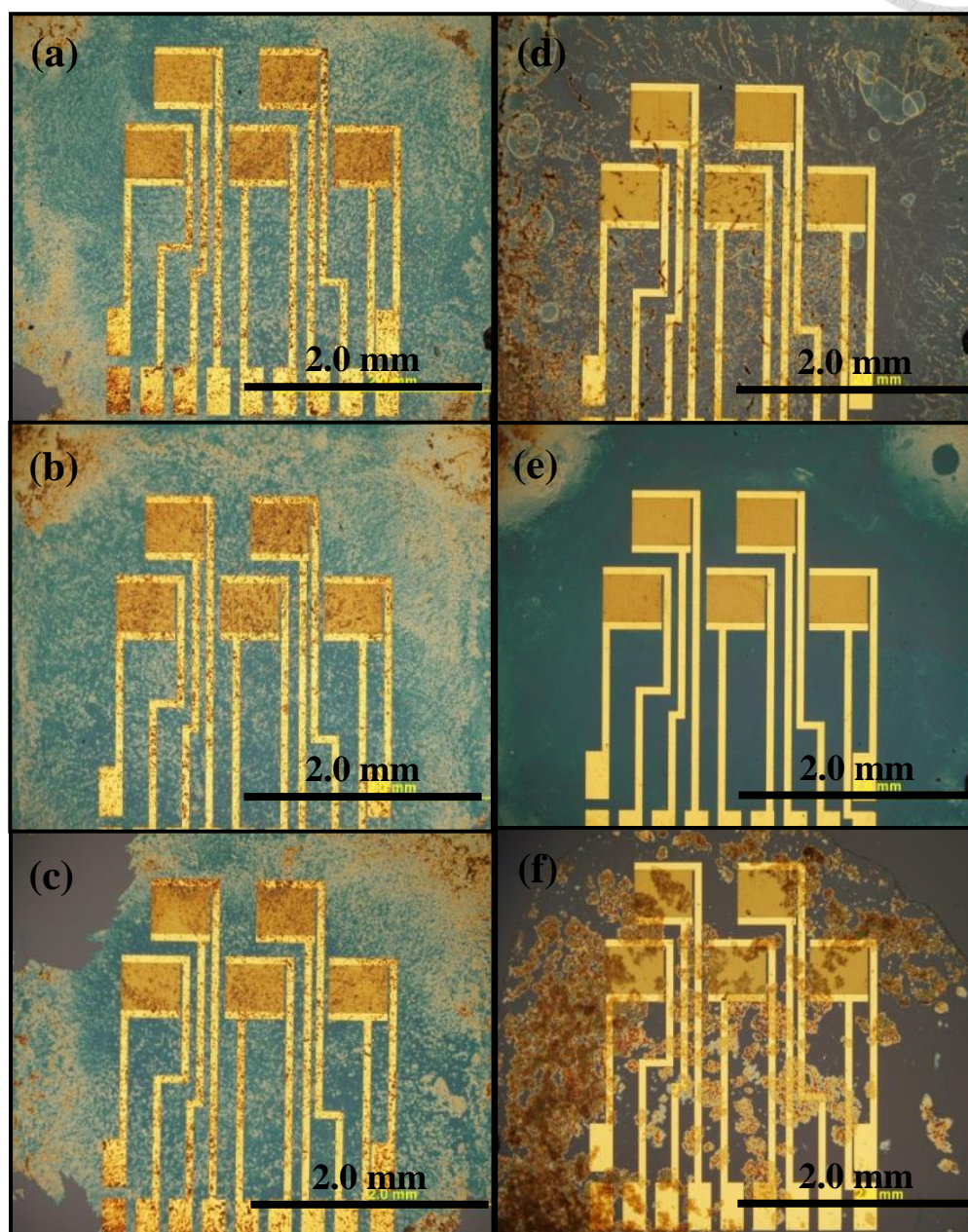
Figure 4-6 The microscope image of GO films with different water/methanol ratios. (a) 10:1, (b) 5:1, (c) 2:1, (d) 1:1, (e) 1:2 and (f) 1:5.
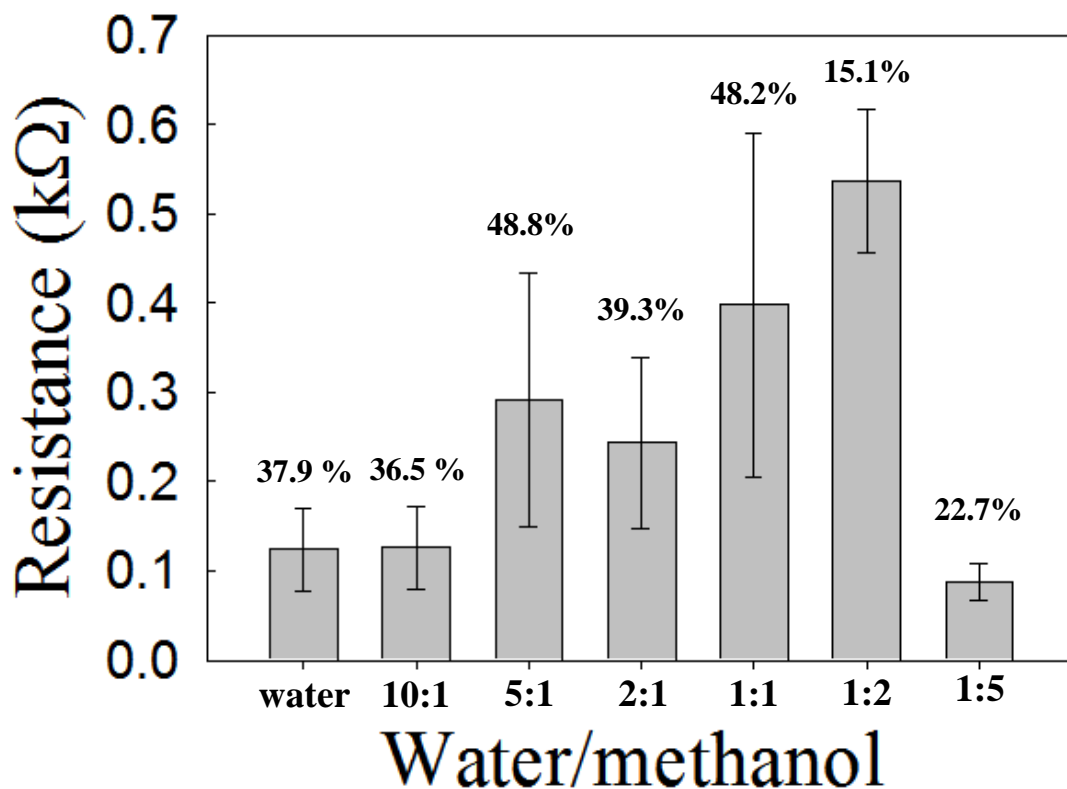
Figure 4-7 The resistance of different water/methanol ratios with error bar.

The values on the top of the column are the standard deviations divided by the respective mean values. The larger value means the larger resistance range and the poorer uniformity of GO thin film. From the results, the uniformity was comparably better at a water/methanol ratio of 1:2. Thus, this experiment result shows a better option for increased coverage and uniformity of GO thin film.

4.2 Reduced process

Currently, the common employed reduction process can generally be categorized into hydrazine and thermal annealing [73]. Although the hydrazine method can

effectively remove the oxide groups on the matrix surface, it cannot remove the carboxyl and carbonyl groups on the sides.   On the other hand, the thermal annealing method can provide graphene with better electrochemical properties.   However, the production process must be conducted at an extremely high temperature, nearly 1000 °C. Therefore, thermal annealing method cannot be considered a cost-effective and rapid method.   This study adopted the use of L-ascorbic acid for the reduction process.   Not only is L-ascorbic acid a moderate and non-toxic biological reductant, but also it can exert its effect under ambient temperature and is suitable for mass production.

4.2.1   Reduced time control

In reduced process, the GO file reduced by the L-Ascorbic acid solution (30 mg/mL) and heated to 90 °C on the hot plate for different time.   After reduced process, the graphene films were washed with D.I. water and dried by the nitrogen.   Figure 4-8 shows the measured resistances with different reduction times.   Result reveals that when the reduction time exceeded 2.5 hours, the resistance lowered and reached to a saturation point.   Thus, the reduction time was established as 3 hours enough for the saturation reduction.   Comparing with the hydrazine vapor and thermal annealing methods, this method is relatively fast and can be carried out under ambient temperature for increasing its mass production potential.

51
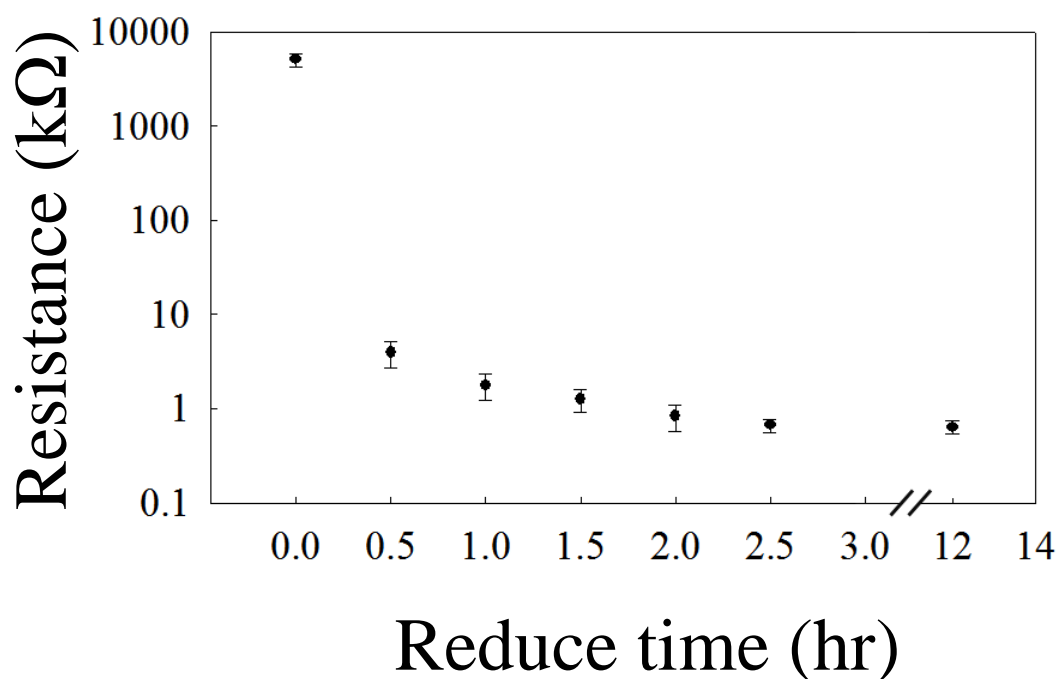
Figure 4-8 rGO resistances with different reduce times.

4.2.2 Raman spectroscopy analysis

Raman spectroscopy is widely used to characterize crystal structure, disorder and defects in graphene-based materials [74]. The reduction process of GO can be proved in Raman spectra by the changes in relative intensity of two main peaks: D band and G band [75]. This method was used to confirm the reduction process. Figure 4-9 shows the Raman spectra of GO powder, GO and reduced GO. The D peak located at 1352 cm^{-1} for GO streams from a defect-induced breathing mode of sp2 rings [76]. It is common to all sp^2 carbon lattice and arises from the stretching of C-C bond. The G peak is at around 1600 cm^{-1} for GO due to the first order scattering of the E2g phonon

52

of sp^2 C atoms. The intensity of the D band is related to the size of the in-plane sp^2 domains [74]. The increase of the D peak intensity indicates forming more sp^2 domains. The relative intensity ratio of both peaks (I_D/I_G) is used to estimate the disorder degree and is inversely proportional to the average size of the sp_2 clusters [74]. From the results shown in Fig 4-9, the D/G intensity ratio for rGO is larger than that for GO (1.05 for rGO and 0.93 for GO). This means that new or more graphitic domains are formed and the sp2 cluster number is increased [76] after reduced process, showing good reduction efficiency [61].
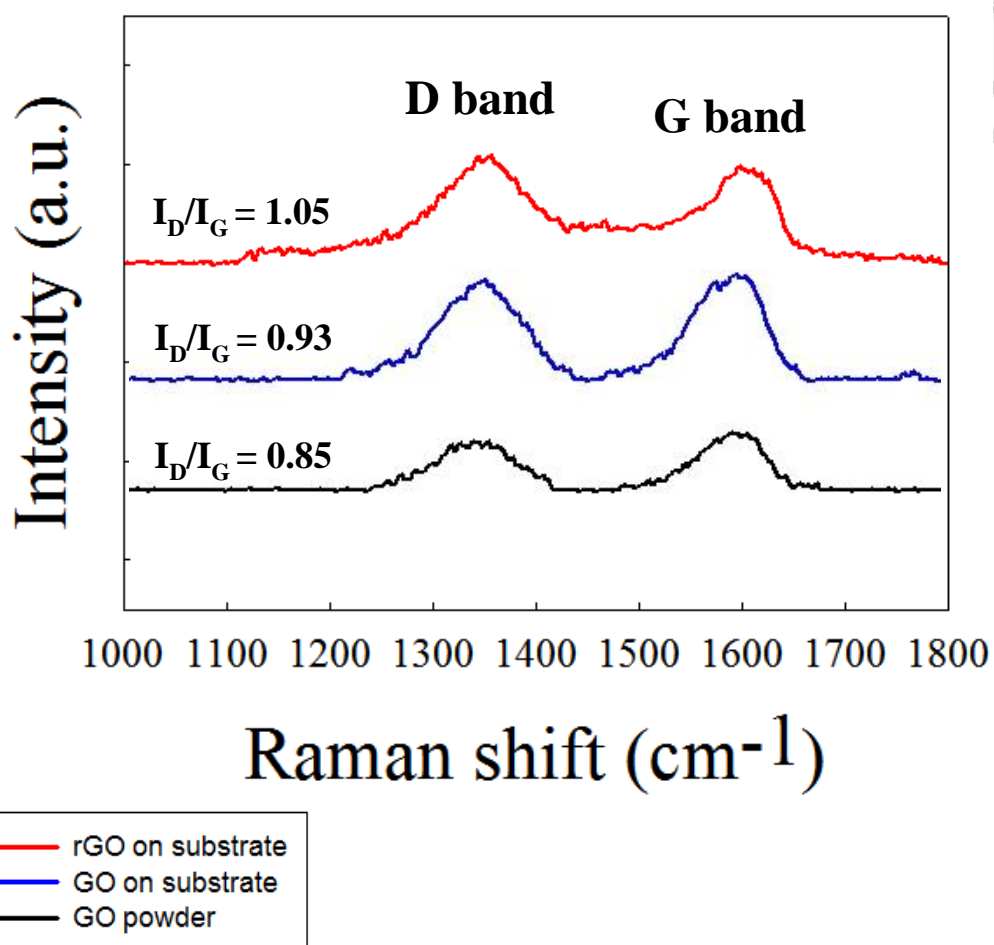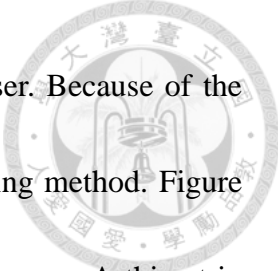
Figure 4-9 Raman spectroscopy analysis for GO powder, GO on substrate and rGO on substrate.

4.3 Spin rate and thickness

GO thin film was prepared by dispersing GO in methanol and water mixture solvents. Films were prepared by varying the rotation rate during spin coating process. The average thickness of thin film was obtained as 14.4 nm, 10.2 nm, 7.2 nm and 6.6 nm at 2000 rpm, 3000 rpm, 4000 rpm and 5000 rpm, respectively. Figure 4-10 shows the SEM image of the GO film prepared under spin coating at 5000 rpm.

The thickness of the thin film was measured by surface analyser. Because of the need to have a relatively film height difference, we used the following method. Figure 4-11 is the analysis figure obtained using Optics-Type Surface Analyser. A thin strip of tape was adhered to the corner of the chip prior to spin coating process and then spin coating process was carried out. After spin coating, the graphene films were dried at 90 °C on a hot plate. Finally, the tape was removed for the thickness measurement. The difference in height between the masked and unmasked regions was taken as the graphene film thickness.
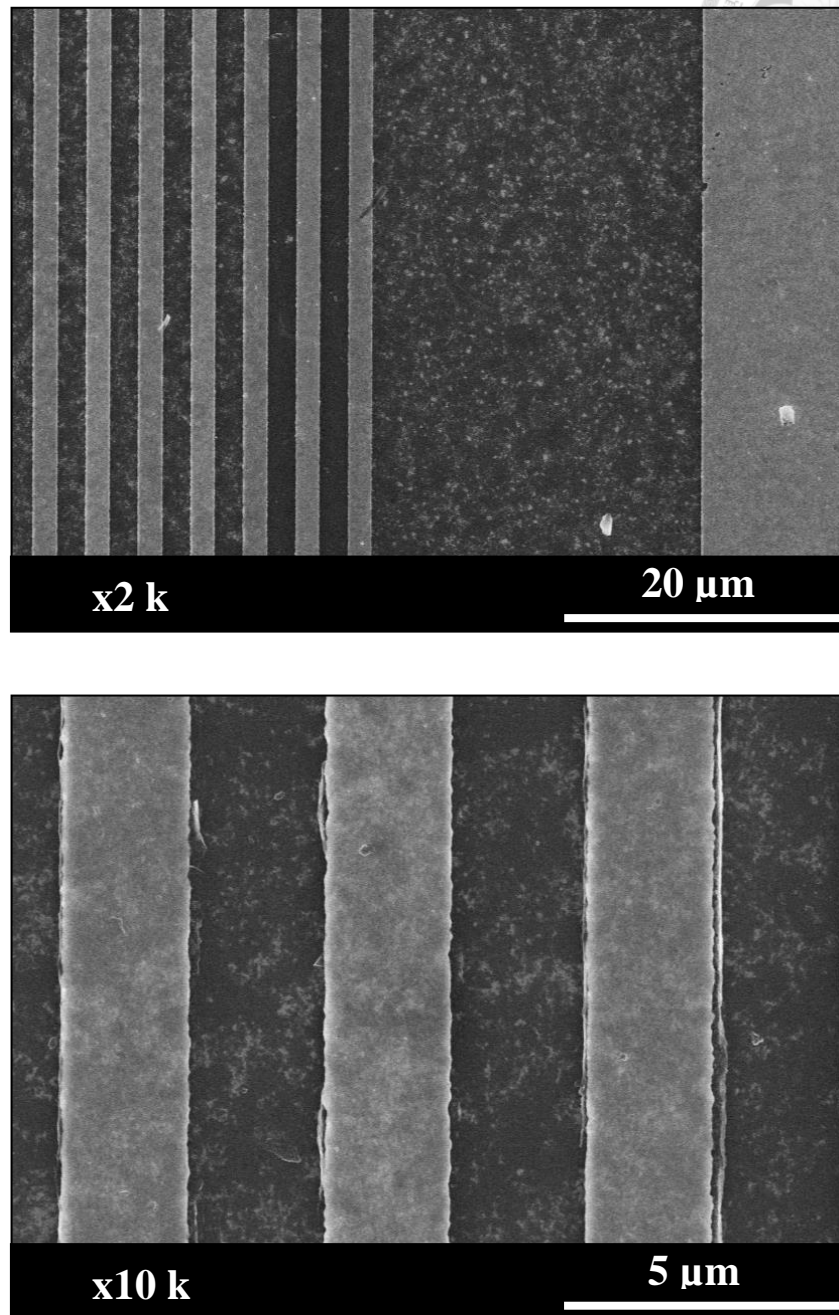
Figure 4-10 SEM image of GO films made with spin coating at 5000 rpm. (a) Image taken at a magnification of 2,000X. (b) Image taken at a magnification of 10,000X.
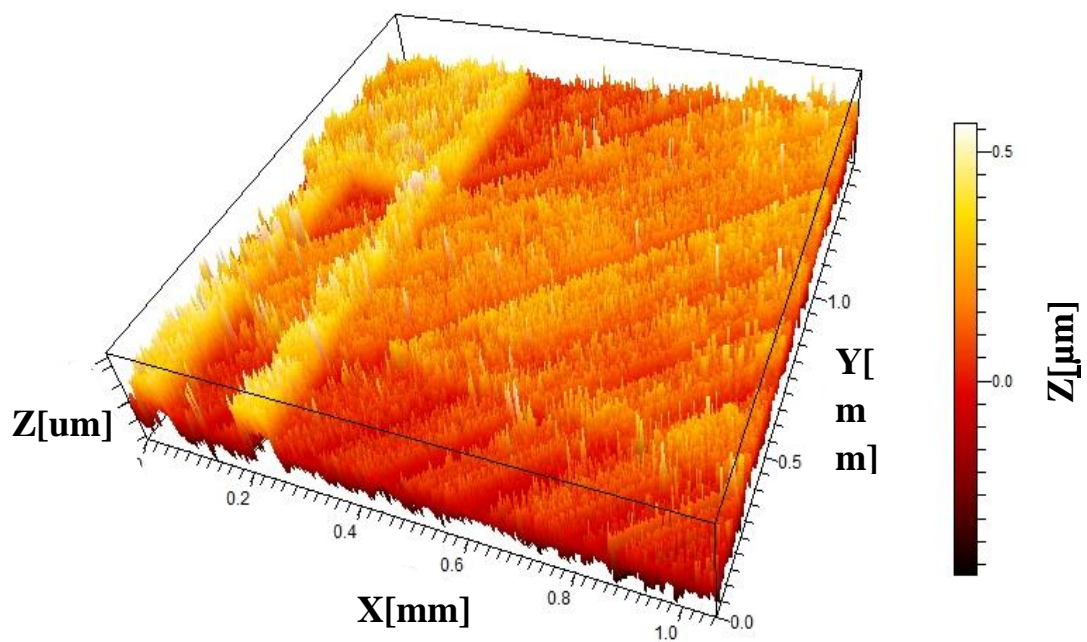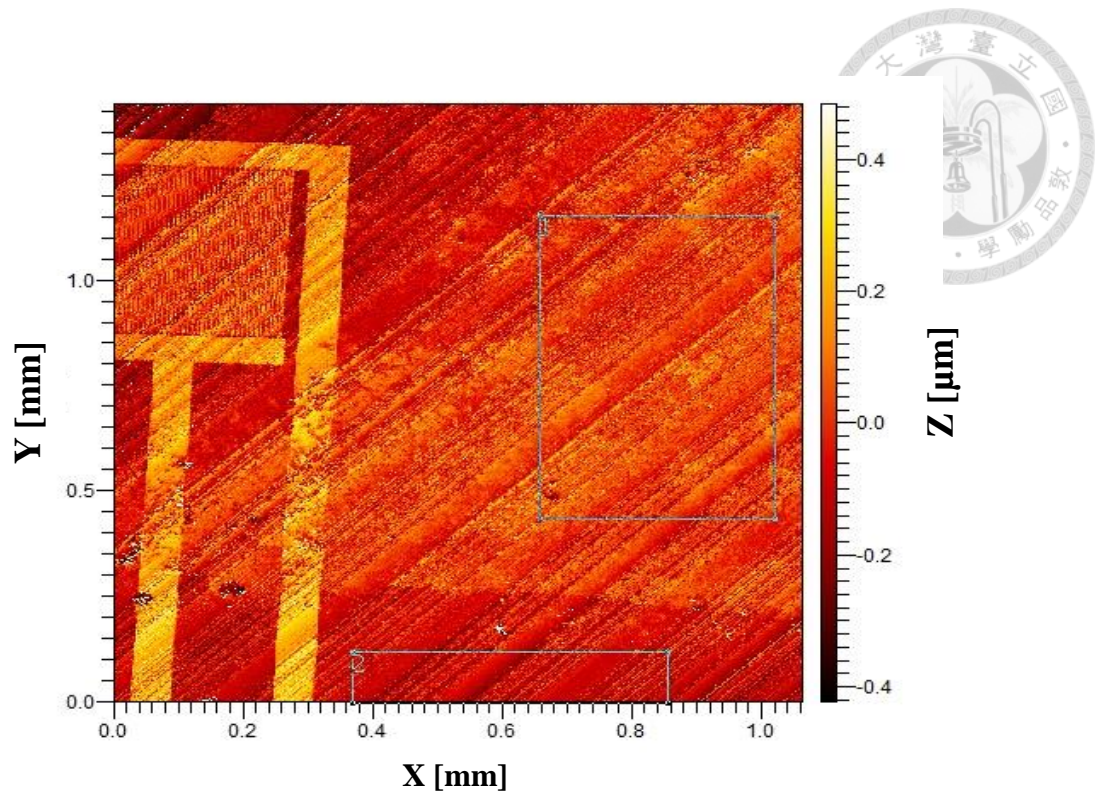
Figure 4-11 GO film thickness analysis by Optics-Type Surface Analyser.

57
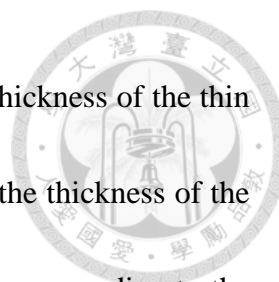
By fitting equation can appear an inverse relation between the thickness of the thin film and the spin rate used at spin coating.　Figure 4-12 represents the thickness of the GO film with different spin rates. The black solid line was fitting line according to the fitting equation described in Section 2.3. Result reveals that A is $1.4\text{x}10^4$ and B is 0.905. The fitting equation is $h = 1.4 \times 10^4 \times \omega^{-0.905}$.　This equation can be a reference parameter for future GO film preparation by spin coating process.　Wherein, B is 0.905 that also complies with the theoretical range described in Sec 2.3.
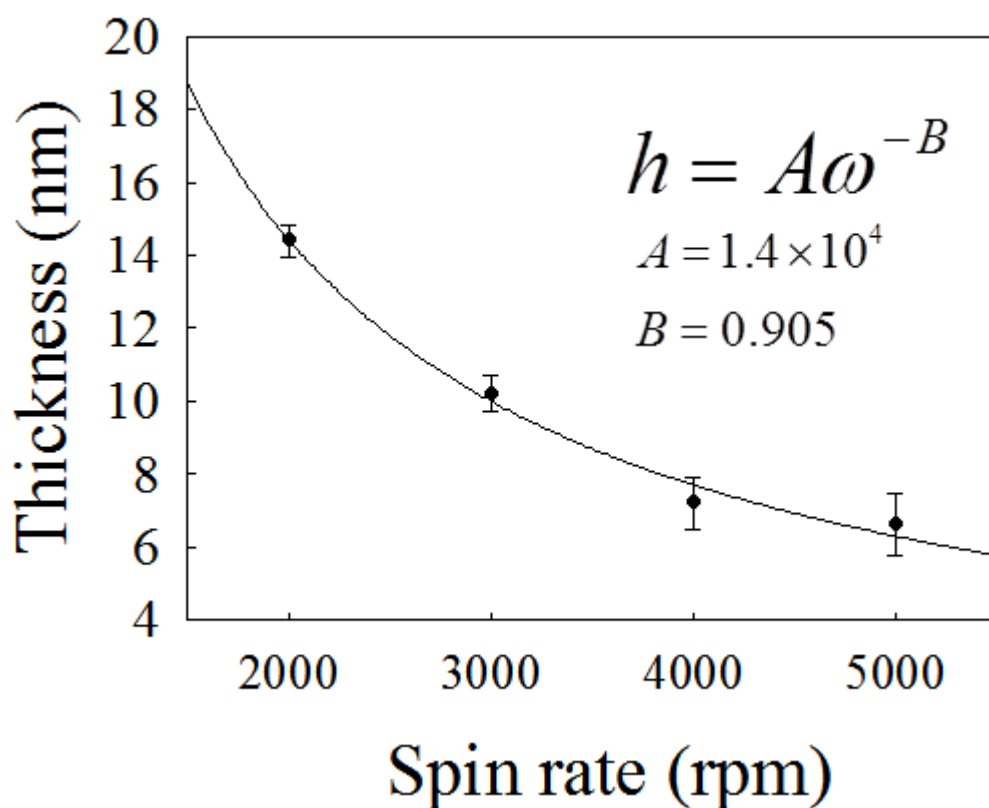
Figure 4-12 GO film thickness as a function of time.

58

4.4　Coverage and uniformity

GO film coverage was improved by the surface hydrophilic treatment. The result demonstrates that surface hydrophilicity should be enhanced to be more hydrophilic for achieving a good coverage.　Besides, the spin rate should be higher than 5000 rpm for the good uniformity of GO film.　Figure 4-13 (a-d) shows the OM image of the spin coated GO film surface without the hydrophilic treatment at 2000 rpm, 3000 rpm, 4000 rpm, and 5000 rpm, respectively.　Figure 4-13 (e-h) shows the OM image of the spin coated GO film surface with the hydrophilic treatment at 2000 rpm, 3000 rpm, 4000 rpm, and 5000 rpm, respectively.　Spin coating process was carried out for three times. Figure 4-14 and 4-15 show the calculated coverage on hydrophobic and hydrophilic surfaces.　As demonstrated, the coverage of spin-coated GO film significant improved by the hydrophilicity treatment.　On the other hand, when the spin rate was increased, the influenced of the edge effect was reduced.
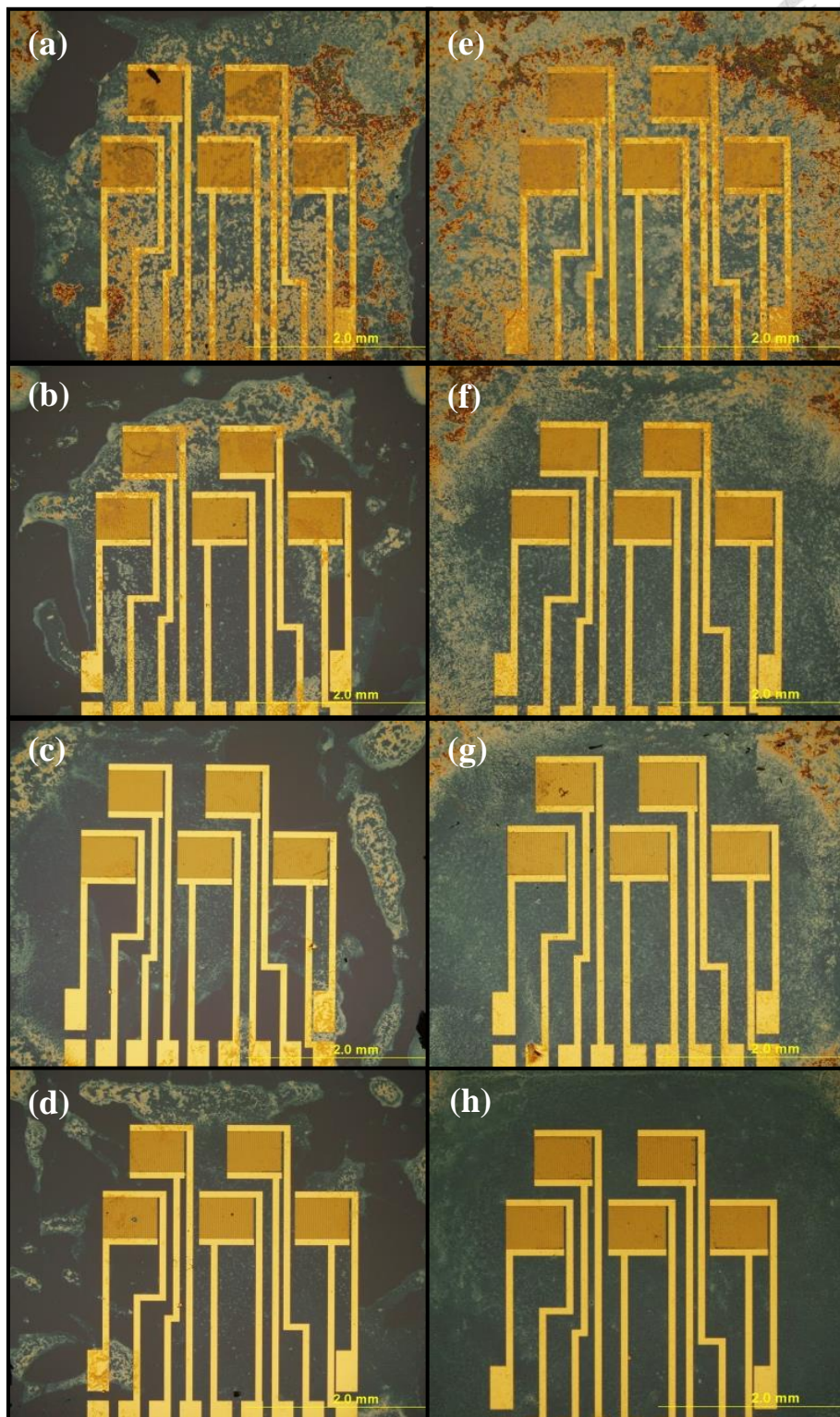
Figure 4-13 The microscope image of GO films with different spin rate on hydrophobic and hydrophilic surface. (a-d) Hydrophobic surface with spin rate 2000, 3000, 4000 and 5000 rpm. (e-h) Hydrophilic surface with spin rate 2000, 3000, 4000 and 5000 rpm.

60
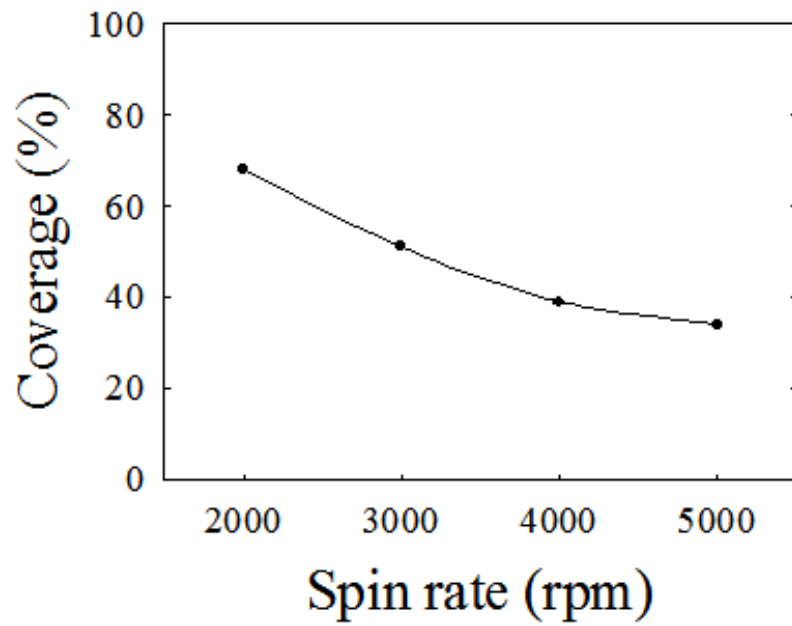
Figure 4-14 Variation of coverage of spin rate on hydrophobic surface.
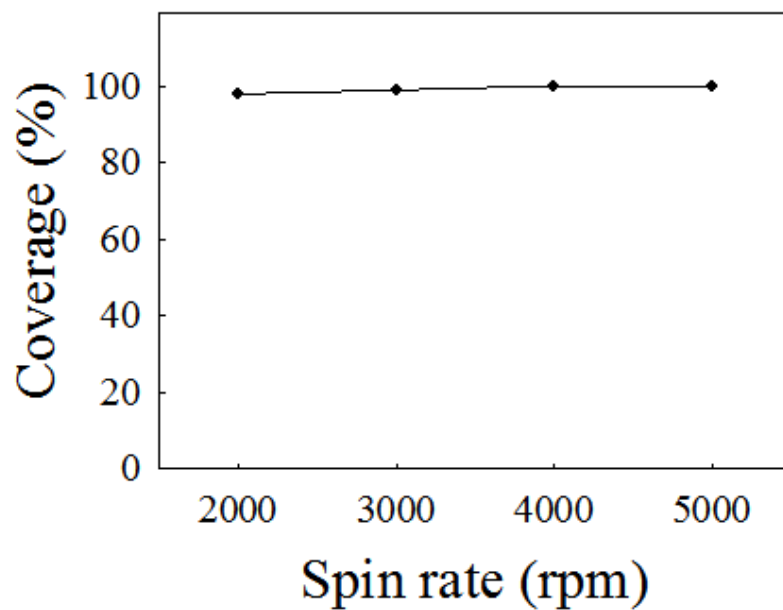
Figure 4-15 Variation of coverage of spin rate on hydrophilic surface.

61
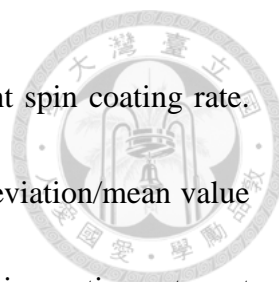
Figure 4-16 shows the resistance of rGO thin film for different spin coating rate. Result reveals that when the spin rate was increased, the standard deviation/mean value was decreased from 54% to 4.3%. This demonstrates that the spin coating rate not only affected film thickness, but influenced uniformly. In addition, because film thickness was reduced when the spin coating rate was increased, the resistance was increased as well.
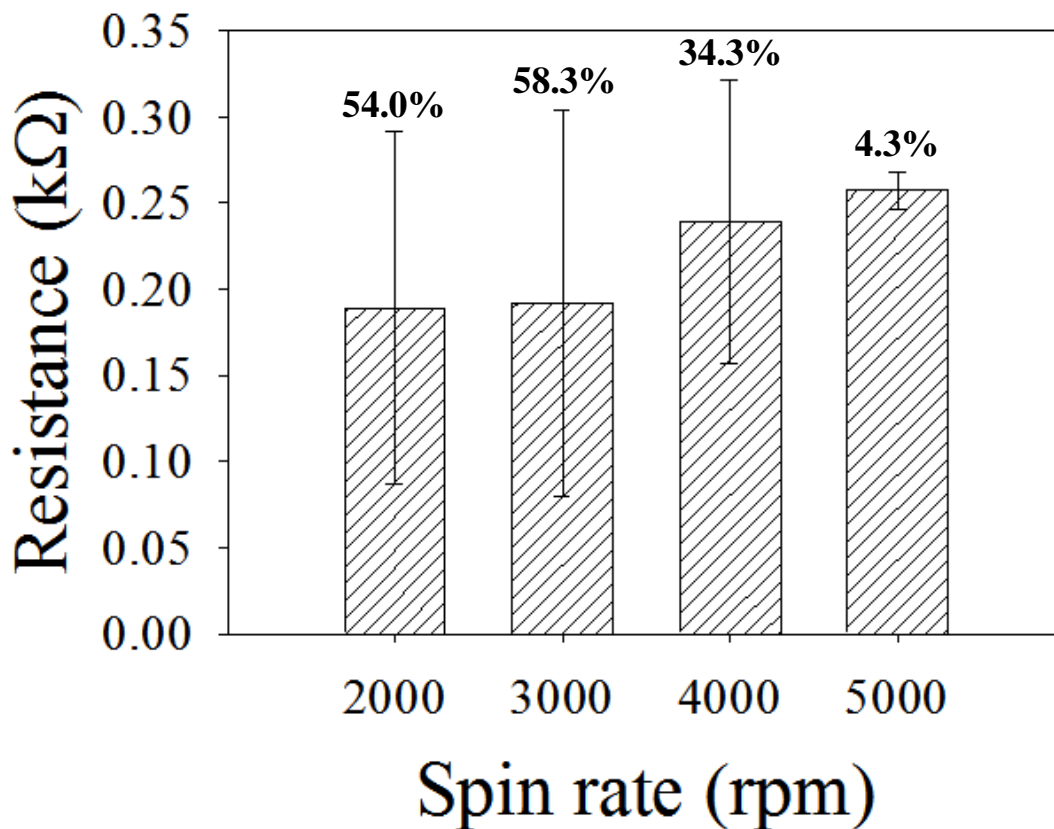
Figure 4-16 Resistance of rGO thin film for different spin rate with error bar.

Moreover, the number of times for spin coating process also influenced uniformity. When the electrode was spin-coated once, the deposited GO was relatively dispersed as shown in Figure 4-17. From the observation, some GO were bridged between electrodes while others were not. The resistance after different spin coating process time was measured and shown in Figure 4-18. When a single spin coating process was carried out, the standard deviation/mean value was extremely high, at 71.6%. However, when twice to three times spin coating processes were employed, the standard deviation/mean value was decreased to 6.6% and 4.3%. This demonstrates that increasing the number of times for spin coating process can increase the uniformity of GO thin film.

63
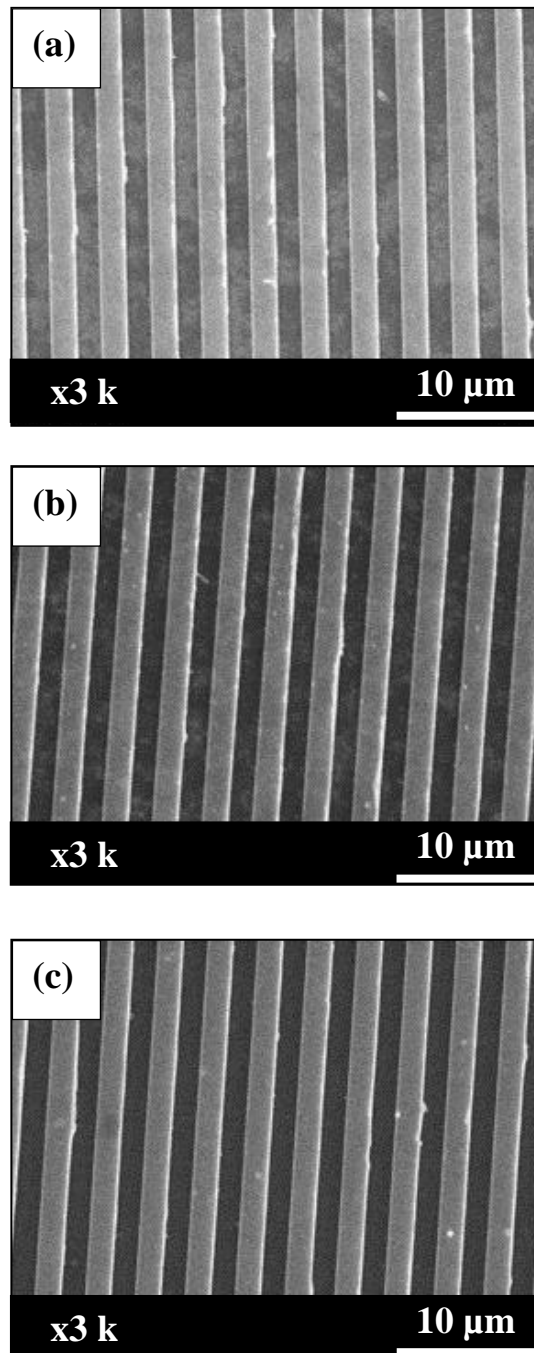
Figure 4-17 SEM image of GO films with different spin times. Image taken at a magnification of 3,000X. (a) Spin coating one times. (b) Spin coating two times. (c) Spin coating three times.
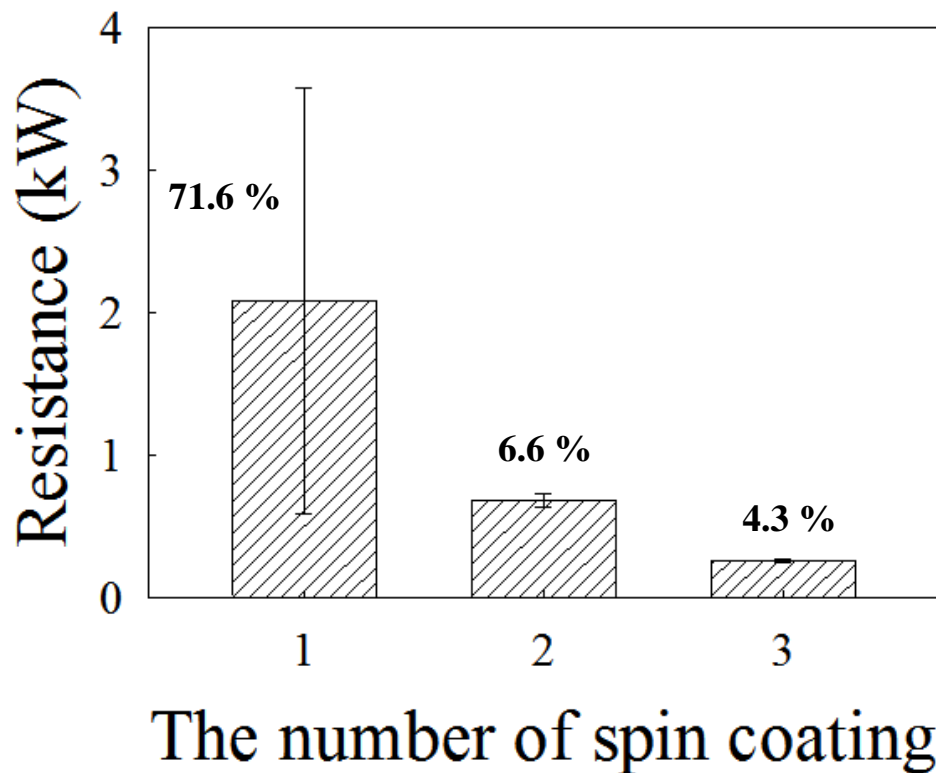
Figure 4-18 Resistance of rGO thin film for different spin times with error bar.

4.5 GO uniformity discussion

After GO was reduced to rGO, resistance measurement was conducted by using a

probe to touch the electrode surface. Even though there was an unstable contact

resistance, the contact resistance may be neglected because the resistance value of rGO

is significantly higher than the contact resistance. For the uniformity of rGO

resistance, the influence are from spin coating rate, hydrophilicity of the matrix, degree

of reduction, selection of GO dispersant, concentration of the GO solution, and the

degree of GO dispersion in the solution.　In this study, we focused on the discussion of the factors of spin rate, matrix hydrophilicity, and parameters of the GO solution.

　As shown in Sec 4.3 and 4.4, when the spin coating rate increased, the thickness of the GO film decreased as well as the edge effect reduced.　When spin coating was conducted at low spin rate, the formed GO film was thicker and aggregated between flaked GO, as shown in the Figure 4-19.　This phenomenon resulted in non-uniform rGO resistance values and the resulting product does not satisfy the requirements of future mass production.　In contrary, when high spin coating rate was used, the GO film was thinner and the sensor area was not affected by the edge effect.　This prevented GO aggregation and provided better uniformity.
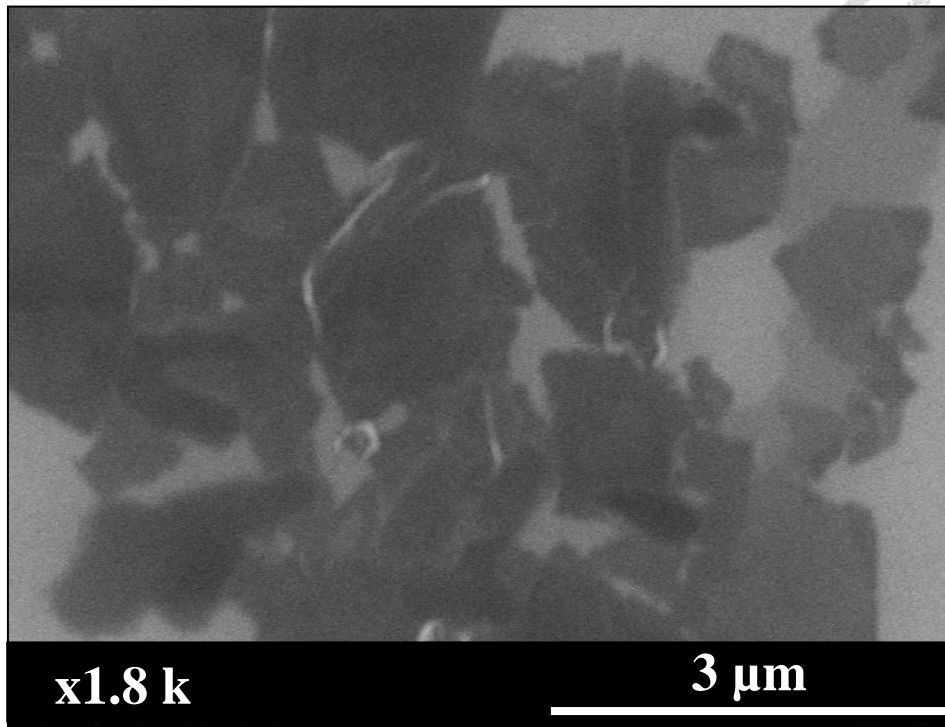
Figure 4-19 SEM image of aggregation GO sheets. Image was taken at a magnification of 18,000X.

Sec. 4.1 and 4.4 discussed the influence of surface treatment on coverage and uniformity. GO is a nano-flake that carries different oxygen containing functional groups on its surface. Thus, GO is a hydrophilic material by itself. When the substrate surface is more hydrophilic, GO thin film will be easier to absorb onto the substrate surface due to van der Waal interactions. Because of it, the GO coverage and yield will increase during mass production. Sec. 4.1.2 described the use of a water/methanol mixture to effectively increase the coverage and uniformity of the GO film. According to the experiment results, a water/methanol ratio of 1:2 provided the

best result.   With a larger water/methanol ratio, where there was significantly more

water, the evaporation of the solvent was too slow and it resulted in aggregation due to

liquid tension.   When the water/methanol ratio was 1:5, where methanol constituted a

larger portion of the mixture, the evaporation speed was too fast and it caused early

evaporation of the solvent befor the adequate coverage of the GO during the spin-up

stage.   Thus, hydrophilicity is not the main factor that affect the results. Rather, the

solvent evaporation rate must also be considered.

4.6   cTnI biomarker detection

The   sensing   structure   after   the   functionalization   process   with

bio-linker/aptamer/block for accomplishing the biochip is shown in figure 4-20(a).

The bio-linkers can be attached onto surface of r-GO via strong interaction between

carbon lattice and pyrenyl group with π-π stacking in basal plane [77]. The cTnI

aptamers are bound to bio-linkers by NHS ester reaction as shown in figure 4-20(b).

The ethanolamine was used to deactivate and to block the remaining NHS ester groups.

The cTnI biomarkers can be captured specifically by cTnI aptamers. Figure 4-20(c)

shows the fluorescent cTnI-aptamer functionalized on the r-GO.

68
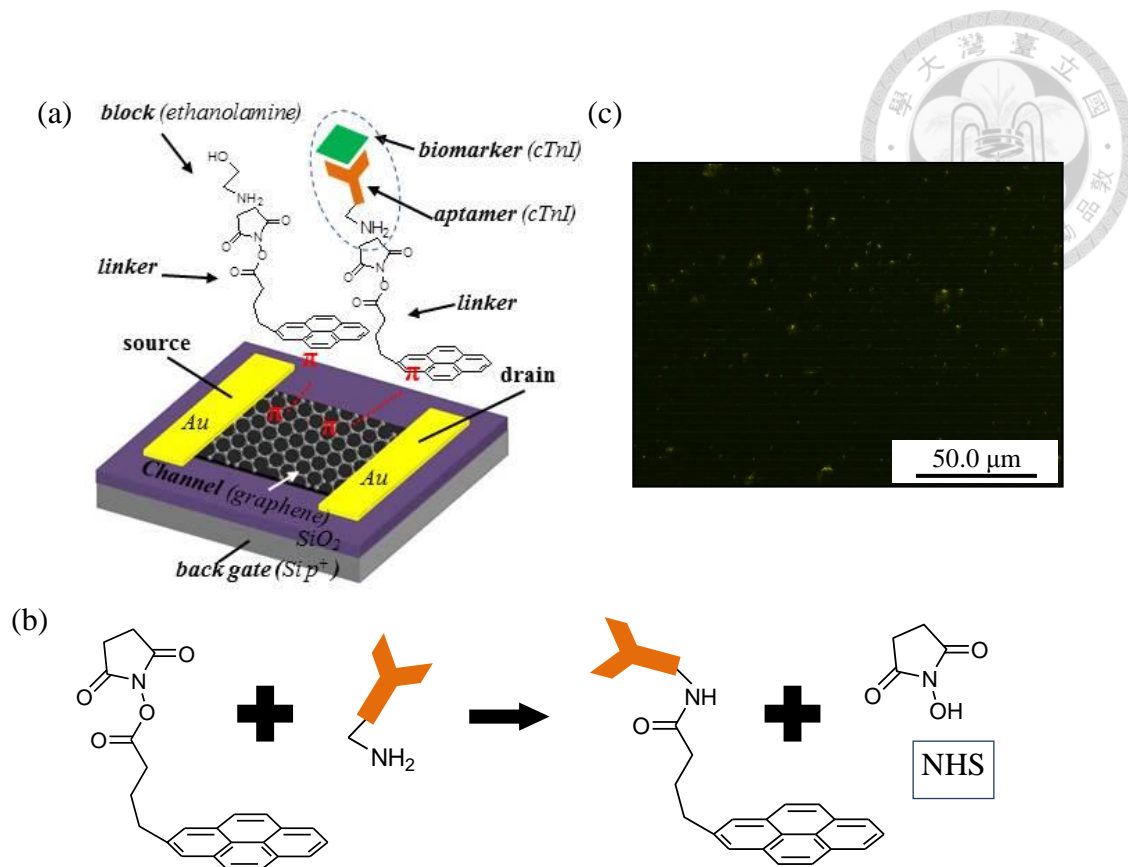
Figure 4-20 (a) Schematic illustration of cTnI aptamer functionalized graphene sensor for detecting of specific cTnI biomarkers; (b) NHS ester reaction process; (c) fluorescent cTnI-aptamer on r-GO.

Clinically, the normal cTnI concentration level in healthy human is lower than 0.4 ng/mL. The level of the high risk of cardiopathy is greater than 2.0 ng/mL. The concentrations of testing solutions in our experiment were 0, 0.2, 1 and 67 ng/mL cTnI biomarkers in PBS solution. The resistance was measured successively as time for 15 minutes at cTnI concentrations of 0, 0.4, 1 and 67 ng/mL respectively. Figure 4-21 shows that the resistance increased and the resistance changed from 0.265 kΩ to 0.318

kΩ for 0 ng/mL, 0.318 kΩ to 0.323 kΩ.for 0.2 ng/mL, 0.323 kΩ to 0.328 kΩ8for 1 ng/mL, and 0.328 kΩ to 0.332 kΩtfor 67 ng/mL. The resistance change was 4.9Ω, 10.2Ω and 14.5Ω from 0 ng/mL to 0.2 ng/mL, 0.2 ng/mL to 1 ng/mL and 1 ng/mL to 67 ng/mL. It indicates that the device is sensitive to ambient environment even if there was no bio-marker in testing solution. However, it has the ability to distinguish 0.2 ng/mL cTnI biomarkers from 0.
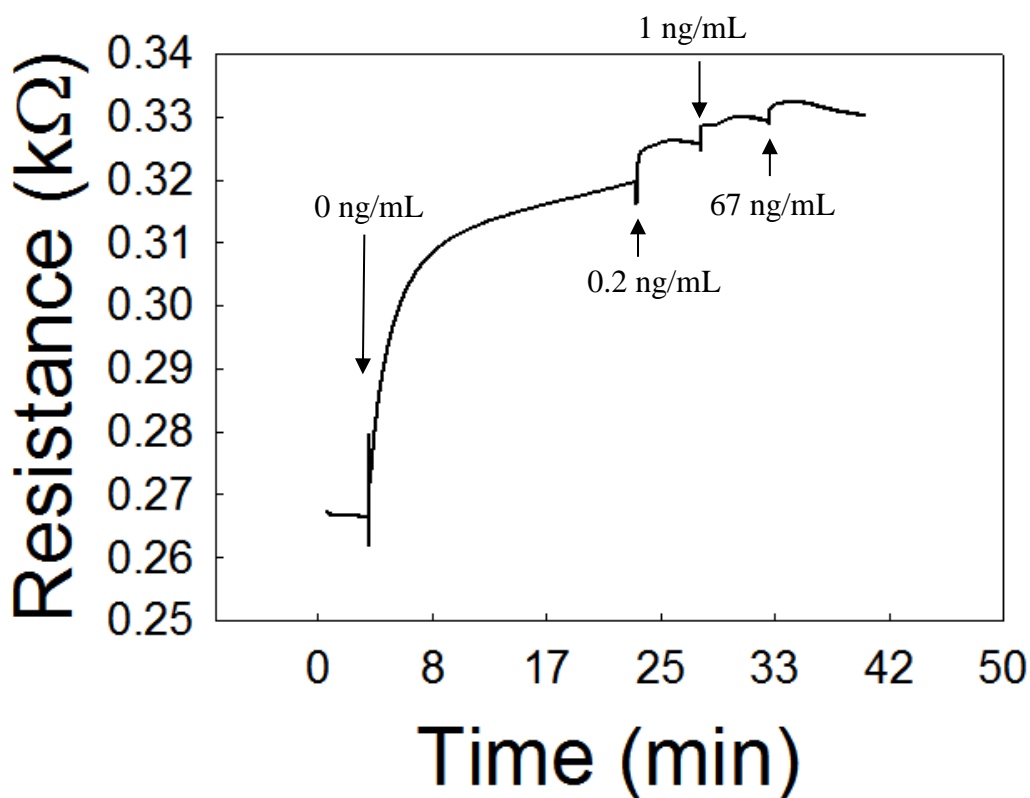
Figure 4-21 The resistance was measured for 15 minutes for cTnI concentrations of 0 ng/mL, 0.2 ng/mL, 1 ng/mL and 67ng/mL.
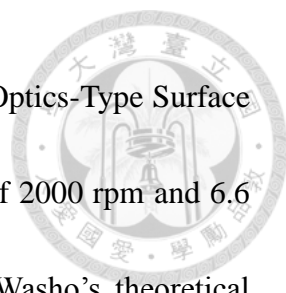
Chapter 5   Conclusions and future works

5.1   Conclusions

In this study, we designed a cardiac Troponin-I biosensor using a micro electro mechanical manufacturing method and demonstrated that spin coating process can be used for providing uniform GO films. Various methods were used to improve the coverage and uniformity of GO films. Herein, two parameters on the hydrophilic modification of surfaces including (1) surface modification and (2) solvent blending were analyzed. For the surface modification method, the substrate was soaked into a piranha solution and a cysteamine solution. The piranha solution caused hydroxylation of the surface of the SiO_2 and made the surface extremely hydrophilic. The contact angle of the SiO_2 surface was reduced from 64.45° to 33.96°. On the other hand, cysteamine formed a SAM on the gold electrode to provide a thin film that increased the hydrophilicity of the gold electrode surface. The contact angle of the gold electrode surface was reduced from 88.9° to 61.14° after cysteamine coating. Both of these methods were proven to effectively enhance surface hydrophilicity. Besides, different solvent blends of water and methanol was used to compare their effects. Result revealed that at a water/methanol ratio of 1:2 shows the best coverage and uniformity of GO thin film.

This research also demonstrated the relationship between spin coating rate and film

71

thickness during the spin coating process by the experiments. By Optics-Type Surface

Analyser, the thickness of the GO film was 14.4 nm at a spin rate of 2000 rpm and 6.6

nm at a spin rate of 5000 rpm. By applying the values to the Washo's theoretical

model, a functional relationship was established between the spin coating rate and GO

film thickness. Regarding the reduction of the graphene, L-Ascorbic acid was

employed and the treatment time of 2.5 hr was sufficient to achieve the saturation

reduction. Furthermore, Raman spectroscopy was used to analyze the rGO after

reduction and to prove reduced GO efficiently. We demonstrated a cTnI

aptamer-functionalized r-GO biosensor to detect cTnI biomarkers with a mass

production method. The developed sensor determined biomarker concentration levels by

resistance variations. The lowest cTnI concentration that the fabricated sensor could

detect is 0.2 ng/mL. Of course, the cTnI aptamer could be replaced with other aptamer

readily to detect other specific disease via this graphene-based bioelectronics sensor in

the future.

5.2   Future works

In this study, we successfully established a technical method to spin coat GO

uniformly on a biochip. Researchers have an identical goal of popularizing a cardiac

Troponin-I biosensor. For the biosensor popularization, the biosensor should be

convenient, rapid, stable, and cost effective.   Besides, the biosensor can also remotely

transport tests results to food agencies for assessment for safeguarding the health of the

public.   Therefore, efforts are being continuously made to product development and

subsequent mass production.

Quality of graphene growth and characteristic control must be addressed, because

graphene was used as the sensing material in the channel of FET.   Its intrinsic

characteristic will affect the electrical property and the biosensor ability.   Therefore,

the stable, uniform and large-scale graphene is necessary to control and develop.   How

to effectively modify the graphene is also an important issue, because the recipes in

each step of the functionalization such as bio-linker binding, bio-aptamer

immobilization, and blocking unbonded sites would affect the sensitivity of biosensor.

Additionally, the specific test is imperative for other cardiac biomarkers.

FET miniaturization and characteristic stability is necessary be emphasized. To

reduce the FET dimensions such as the thickness of dielectric layer as well as the width

and length of graphene strip is an absolute work in the future.   Thinner dielectric layer

could make the Dirac point detectable for verifying the doing effect.   Narrower and

shorter graphene strip could decrease the defect concentration and hence open the band

gap.   Integration of signal processing circuit also has to be developed.   The I_D-V_{GS}

curve was measured by semiconductor parameter analyzer.   Although the

measurement is simple and fast, the apparatus is not inconvenient and costly for

point-of-care. In the future, the apparatus could be simplified and minimized by the

electrical circuit design.
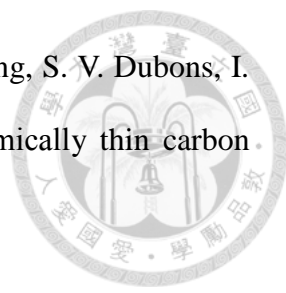
Reference
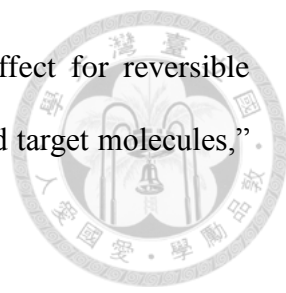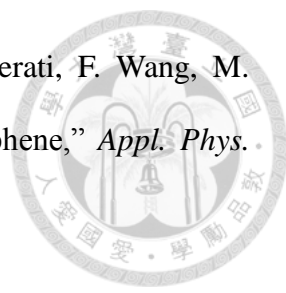
[1] Mayo Clinic. (2014, July). Heart disease, definition. [Online]. Available: http://www.mayoclinic.org/

[2] Patient Info. (2016, May). Acute coronary syndrome. [Online]. Available: http://patient.info/

[3] A. M. Gordon, E. Homsher, and M. Regnier, "Regulation of contraction in striated muscle," *Physiological Reviews*, vol. 80, no. 2, pp.853-924, 2000.

[4] J. L. McDonough and J. E. V. Eyk, "Developing the next generation of cardiac markers: disease-induced modifications of troponin I," *Prog. Cardiovasc. Dis.*, vol. 47, pp. 207-216, 2004.

[5] V. S. Mahajan and P. Jarolim, "How to interpret elevated cardiac troponin levels," *Circulation*, vol. 124, pp. 2350-2354, 2011.

[6] P. Zuo, X. Li, D. C. Dominguez, and B.-C. Ye, "A PDMS/paper/glass hybrid microfluidic biochip integrated with aptamer-functionalized graphene oxide noano-biosensors for one-step multiplexed pathogen detection," *Lab Chip*, vol. 13, pp. 3921-3928, 2013.

[7] W. U. Dittmer, T. H. Evers, W. M. Hardeman, W. Huijnen, R. Kamps, P. d. Kievit, J. H. M. Neijzen, J. H. Nieuwenhuis, M. J. J. Sijbers, D. W. C. Dekkers, M. H. Hefti, and M. F. W. C. Martens, "Rapid, high sensitivity, point-of- care test for cardiac troponin based on optomagnetic biosensor," *Clin. Chim. Acta*, vol. 411, pp. 868-873, 2010.

[8] NewLife BioChemEX LLC. (2012). ELISA. [Online]. Available: http://www.nlbiochemex.com/

[9] V. Bhalla, S. Carrara, P. Sharma, Y. Nangia, and C. R. Suri, "Gold nanoparticles mediated label-free capacitance detection fo cardiac troponin I," *Sensor. Actuator. B*, vol. 161, pp. 761-768, 2012.

[10] A. Periyakaruppan, R. P. Gandhiraman, M. Meyyappan and, J. E. Koehne, "Label-free detection of cardiac troponin-I using carbon nanofiber based nanoelectrode arrays," *Anal. Chem.*, vol. 85, pp. 3858-3863, 2013.

[11] J. Wu, D. M. Cropek, A. C. West, and S. Banta, "Development of a troponin I biosensor using a peptide obtained through phage display," *Anal. Chem.*, vol. 82, pp. 8235-8243, 2010.

[12] W.-J. Kim, B. K. Kim, A. Kim, C. Huh, C. S. Ah, K.-H. Kim, J. Hong, S. H. Park, S. Song, J. Song, and G. Y. Sung, "Response to cardiac markers in human serum analyzed by guided-mode resonance biosensor," *Anal. Chem.*, vol. 82, pp. 9686-9693, 2010.

[13] W.-Y. Wu, Z.-P. Bian, W. Wang, W. Wang, and J.-J. Zhu, "PDMS gold nanoparticle composite film-based silver enhanced colorimetric detection of cardiac troponin I," *Sensor. Actuator. B*, vol. 147, pp. 298-303, 2010.

[14] Y.-C. Kwon, M.-G. Kim, E.-M. Kim, Y.-B. Shin, S.-K. Lee, S. D. Lee, M.-J. Cho, and H.-S. Ro, "Development of a surface plasmon resonance-based immunosensor for the rapid detection of cardiac troponin I," *Biotechnol. Lett.*, vol. 33, pp. 921-927, 2011.

[15] Z. R. Guo, C. R. Gu, X. Fan, Z. P. Bian, H. F. Wu, D. Yang, N. Gu, and J. N. Zhang, "Fabrication of anti-human cardiac troponin I immunogold nanorods for sensing acute myocardial damage," *Nanoscale Res. Lett.*, vol. 4, pp. 1428-1433, 2009.

[16] M. Shan, M. Li, X. Qiu, H. Qi, Q. Gao, and C. Zhang, "Sensitive electrogenerated chemiluminescence peptide-based biosensor for the determination of troponin I

with gold nanoparticles amplification," *Gold Bull.*, vol. 47, pp. 57-64, 2014.

[17] P. K. Ang, A. Li, M. Jaiswal, Y. Wang, H. W. Hou, J. T. L. Thong, C. T. Lim, and K. P. Loh, "Flow sensing of single cell by graphene transistor in a microfluidic channel," *Nano, Lett.*, vol. 11, pp. 5240-5246, 2011.

[18] R. X. He, P. Lin, Z. K. Liu, H. W. Zhu, X. Z. Zhao, H. L. W. Chan, and F. Yan, "Solution-gated graphene field effect transistors integrated in microfluidic systems and used for flow velocity detection," *Nano Lett.*, vol. 12, pp. 1404-1409, 2012.

[19] L. C. Clark, Jr. and C. Lyons, "Electrode systems for continuous monitoring in cardiovascular surgery", *Ann. Ny. Acad. Sci.*, vol. 102, pp. 29-45, 1962.

[20] S. J. Updike and G. P. Hicks, "The enzyme electrode," *Nature*, vol. 214, pp. 986-988, 1967.

[21] G. Saltzgaber, P. Wojcik, T. Sharf, M. R Leyden, J. L Wardini, C. A Heist, A. A Adenuga, V. T Remcho, and E. D Minot, "Scalable graphene field-effect sensors forspecific protein detection," *Nanotechnology,* vol. 24, 355502, 2013.

[22] M. Ueda, Y. Takamura, Y. Horiike, and Y. Baba, "Molecular detection in an microfluidic device by streaming current measurement," *JPN. J. APPL. PHYS.*, vol. 41, pp. L1275-L1277, 2002.

[23] D. C. Martins, V. Chu, D. M. F. Prazeres, and J. P. Conde, "Electrical detection of DNA immobilization and hybridization by streaming current measurements in microchannels," *Appl. Phys. Lett.*, vol. 99, pp. 183702, 2011.

[24] D. L. Robertson and G. F. Joyce, "Selection in vitro of an RNA enzyme that specifically cleaves single-stranded DNA," *Nature*, vol. 344, pp. 467-468, 1990.
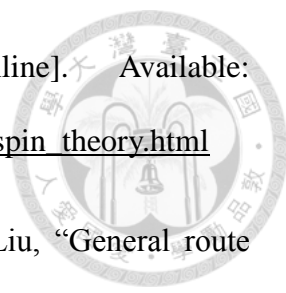
[25] K. S. Novoselov, A. K. Geim, S. V. Morozov, D. Jiang, Y. Zhang, S. V. Dubons, I. V. Grigorieva, and A. A. Firsov, "Electric field effect in atomically thin carbon films," *Science*, vol. 306, pp. 666-669, 2004.

[26] C. Lee, X. Wei, J. W. Kysar, and J. Hone, "Measurement of the elastic properties and intrinsic strength of monolayer graphene," *Science*, vol. 321, pp. 385-388, 2008.

[27] R. R. Nair, P. Blake, A. N. Grigorenko, K. S. Novoselov, T. J. Booth, T. Stauber, N. M. R. Peres, and A. K. Geim, "Fine structure constant defines visual transparency of graphene," *Science*, vol. 320, pp. 1308, 2008.

[28] R. Raccichini, A. Varzi, S. Passerini, and B. Scrosati, "The role of graphene for electrochemical energy storage," *Nat. Mater.*, vol. 14, pp. 271-279, 2015.

[29] F. Schedin, A. Geim, S. Morozov, E. Hill, P. Blake, M. Katsnelson, and K. Novoselov, " Detection of individual gasmolecules adsorbed on graphene," *Nat. Mater.*, vol. 6, pp. 652-655, 2007.

[30] N. Mohanty and V. Berry, "Graphene-based single-bacterium resolution biodevice and DNA transistor: interfacing graphene derivatives with nanoscale and microscale biocomponents," *Nano. Lett.*, vol. 8, pp. 4469-4476, 2008.

[31] W. S. Hummers and R. E. Offeman, "Preparation of graphitic oxide," *J. Am. Chem. Soc.*, vol. 80, p. 1339, 1958.

[32] P. Lia, B. Zhangb and, T. Cuib, "Towards intrinsic graphene biosensor: A label-free, suspended single crystalline graphene sensor for multiplex lung cancer tumor markers detection," *Biosens. Bioelectron.*, vol. 72, pp. 168-174, 2015.
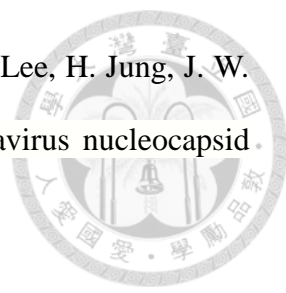
[33] P.-J. J. Huang, R. Kempaiah, and J. Liu, "Synergistic pH effect for reversible shuttling aptamer-based biosensors between graphene oxide and target molecules," *J. Mater. Chem.*, vol. 21, pp. 8991-8993, 2011.

[34] L. Jiang, R. Yuan, Y. Chai, Y. Yuan, L. Bai, and Y. Wang, "Aptamer-based highly sensitive electrochemical detection of thrombin via the amplification of graphene," *Analyst.*, vol. 137, pp. 2415-2420, 2012.

[35] Y. Wang, Y. Xiao, X. Ma, N. Li, and X. Yang, "Label-free and sensitive thrombin sensing on a molecularly grafted aptamer on graphene," *Chem. Commun.*, vol. 48, pp. 738-740, 2012.

[36] A. Reina, X. Jia, J. Ho, D. Nezich, H. Son, V. Bulovic, M. S. Dresselhaus, and J. Kong, "Large area, few-layer graphene films on arbitrary substrates by chemical vapor deposition," *Nano. Lett.*, vol. 9, pp. 30-35, 2009.

[37] W. Cai, A. L. Moore, Y. Zhu, X. Li, S. Chen, L. Shi, and R. S. Ruoff , "Thermal transport in suspended and supported monolayer graphene grown by chemical vapor deposition," *Nano. Lett.*, vol. 10, pp. 1645-1651, 2010.

[38] X. Li, Y. Zhu, W. Cai, M. Borysiak, B. Han, D. Chen, R. D. Piner, L. Colombo, and R. S. Ruoff, "Transfer of large-area graphene films for high-performance transparent conductive electrodes," *Nano. Lett.*, vol. 9, pp. 4359-4363, 2009.

[39] J. D. Wood, G. .P Doidge, E. A. Carrion, J. C. Koepke, J. A. Kaitz, I. Datye, A. Behnam, J. Hewaparakrama, B. Aruin, Y. Chen, H. Dong, R. T. Haasch, J. W. Lyding, and E. Pop, "Annealing free, clean graphene transfer using alternative polymer scaffolds," *Nanotechnology*, vol. 26, pp. 055302, 2015.
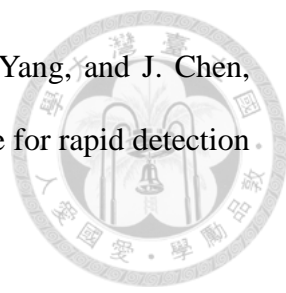
[40] W. Regan, N. Alem, B. Alemán, B Geng, Ç. Girit, L. Maserati, F. Wang, M. Crommie, and A. Zettla, "A direct transfer of layer-area graphene," *Appl. Phys. Lett.*, vol. 96, pp. 102-113, 2010.

[41] L. J. Cote, F. Kim, and J. Huang, "Langmuir-Blodgett assembly of graphite oxide single layers," *J. Am. Chem. Soc.*, vol. 131, pp. 1043-1049, 2009.

[42] M. Musoddiq Jaafar, G. P. M. K. Ciniciato, S. A. Ibrahim, S. M. Phang, K. Yunus, A. C. Fisher, M. Iwamoto, and P. Vengadesh, "Preparation of a three-dimensional reduced graphene oxide film by using the Langmuir–Blodgett method," *Langmuir.*, vol. 31, pp. 10426-10434, 2015.

[43] L. J. Cote, J. Kim, V. C. Tung, J. Luo, F. Kim, and J. Huang, "Graphene oxide as surfactant sheets," *Pure. Appl. Chem.*, vol. 83, pp. 95-110, 2011.

[44] J. Chang, S. Mao, Y. Zhang, S. Cui, G. Zhou, X. Wu, C. H. Yang, and J. Chen, "Ultrasonic-assisted self-assembly of monolayer graphene oxide for rapid detection of Escherichia coli bacteria," *Nanoscale*, vol. 5, pp. 3620-3626, 2013.

[45] S. Bykkam, K.V. Rao, C. S. Chakra, V. Rajendar, R. N. Kumar and J. Ananthaiah, "Graphene oxide thin films: A simple profilometer for film thickness measurement," *IJEAT.,* vol. 2, pp. 2249-8958, 2013.

[46] B. J. Tarasevich, J. Liu, M. Sarikaya and I. A. Akasy, "Inorganic gels with nanometer-sized particles," *Mat. Res. Soc. Symp. Proc.*, vol. 121, pp.225-237, 1988.

[47] A. G. Emslie, F. T. Bonner, and L. G. Peck, "Flow of a viscous liquid on a rotating disk," *Appl. Phys.*, vol. 29, pp. 858-862, 1958.

[48] D. Meyerhofer, "Characteristics of resist films produced by spinning," *J. Appl. Phys.*, vol. 49, pp. 3993, 1978.

[49] Brewer Science. (1997). Spin coating theory. [Online]. Available: http://www.brewerscience.com/spin-coating-theory

[50] N. Sahu, B. Parija, and S. Panigrahi, "Fundamental understanding and modeling of spin coating process: A review," *Indian J. Phys.*, vol. 83, pp. 493-502, 2009.

[51] G. A. Luurtsema, "Spin coating for rectangular substrates," M.S. thesis, Dept. Elec. Eng. And Com. Sci., Univ. CA., Berkeley, 1997.

[52] 蘇清源，"物理專文:石墨烯氧化物之特性與應用前景"，物理雙月刊，第 33 卷，第 2 期，第 163-167 頁，2011。

[53] D. E. Bornside, C. W. macosko, and L. E. Scriven, "Spin coating: Onedimensional model," *J. Appl. Phys.*, vol. 66, pp. 5185, 1989.

[54] Y. S. Kim, H. S. Jung, T. Matsuura, H. Y. Lee, T. Kawai, and M. B. Gu, "Electrochemical detection of 17β-estradiol using DNA aptamer immobilized gold electrode chip," *Biosens Bioelectron*, vol. 22, pp. 2525-2531, 2007.

[55] B.D. Washo, "Rheology and modeling of the spin coating process," *IBM J. Res. Dev.*, vol. 21, pp. 190-198, 1977.

[56] D. P. Birnie III, S. K. Hau, D. S. Kamber, and D. M. Kaz, "Effect of ramping-up rate on film thickness for spin-on processing," *J. Mater. Sci.*, vol. 16, pp. 715-720, 2005.

[57] Georgia Tech. (2004, Jun.). Spin theory. [Online]. Available: http://www2.ece.gatech.edu/research/labs/vc/packaging/theory/spin_theory.html

[58] Y. Guo, C. Di, H. Liu, J. Zheng, L. Zhang, G. Yu, and Y. Liu, "General route toward patterning of graphene oxide by a combination of wettability modulation and spin-coating," *Acs Nano*, vol. 4, pp. 5749-5754, 2010.

[59] Ossila enabling innovative electronics. (2016). Spin coating: A guide to theory and techniques. [Online]. Available: http://www.ossila.com/pages/spin-coating

[60] M. Wirde and U. Gelius, "Self-assembled monolayers of cystamine and cysteamine on gold studied by XPS and voltammetry," *Langmuir*, vol. 15, pp. 6370–6378, 1999.

[61] X. Zhu, Q. Liu, X. Zhu, C. Li, M. Xu, and Y. Liang, "Reduction of graphene oxide via ascorbic acid and its application for simultaneous detection of dopamine and ascorbic acid," *Int. J. Electrochem. Sci.*, vol. 7, pp. 5172-5184, 2012.

[62] J. Vivekananda, J. L. Kiel, "Anti-francisella tularensis DNA aptamers detect tularemia antigen from different subspecies by aptamer-linked immobilized sorbent assay," *Lab. Invest.*, vol. 8, pp, 610-618, 2006.

[63] E. Baldrich, J. L. Acero, G. Reekmans, W. Laureyn, C. K. O'Sullivan, "Displacement enzyme linked aptamer assay," *Anal. Chem.*, vol. 77, pp. 4774-4874, 2005.

[64] B. Strehlitz, N. Nikolaus, R. Stoltenburg, "Protein detection with aptamer biosensors," *Sensors*, vol. 8, pp. 4296-4307, 2008.

[65] D. G. Ahn, I. J. Jeon, J. D. Kim, M. S. Song, S. R. Han, S. W. Lee, H. Jung, J. W. Oh, "RNA aptamer-based sensitive detection of SARS coronavirus nucleocapsid protein," *Analyst*, vol. 134, pp. 1896-1901, 2009.

[66] D. L. Robertson, G. F. Joyce, "Selection in vitro of an RNA enzyme that specifically cleaves single-stranded DNA," *Nature*, vol. 344, pp. 467-468, 1990.

[67] A. D. Ellington, J. W. Szostak, "In vitro selection of RNA molecules that bind specific ligands," *Nature*, vol. 346, pp. 818-822, 1990.

[68] C. Tuerk, L. Gold, "Systematic evolution of ligands by exponential enrichment: RNA ligands to bacteriophage T4 DNA polymerase," *Science*, vol. 249, pp. 505-510, 1990.

[69] R. E. Wang, H. Wu, Y. Niu, J. Cai, "Improving the stability of aptamers by chemical modification," *Curr. Med. Chem.*, vol. 18, pp. 4126-4138, 2011.

[70] S. Balamurugan, A. Obubuafo, S. A. Soper, D. A. Spivak, "Surface immobilization methods for aptamer diagnostic applications," *Anal. Bioanal. Chem.*, vol. 390, pp. 1009-1021, 2008.

[71] J. Zhang, H. Yang, G. Shen, P. Cheng, J. Zhang, and S. Guo, "Reduction of graphene oxide via L-ascorbic acid," *Chem. Commun.*, vol. 46, pp. 1112-1114, 2010.

[72] L. Yang, Y. Li, C. L. Griffis, and M. G. Johnson, "Interdigitated microelectrode (IME) impedance sensor for the detection of viable Salmonella typhimurium," *Biosens. Bioelectron.*, vol. 19, pp. 1139-1147, 2004.

[73] J. Chang, S. Mao, Y. Zhang, S. Cui, G. Zhou, X. Wu, C.-H. Yang, and J. Chen, "Ultrasonic-assisted self-assembly of monolayer graphene oxide for rapid detection of Escherichia coli bacteria," *Nanoscale,* vol. 5, p. 3620, 2013.

[74] S. Gurunathan, J. W. Han, E. S. Kim, J. H. Park, and J.-H. Kim, "Reduction of graphene oxide by resveratrol: a novel and simple biological method for the synthesis of an effective anticancer nanotherapeutic molecule," *Int. J. Nanomedicine*, vol. 10, pp. 2951-2969, 2015.

[75] A. Jorio, M. Dresselhaus, R. Saito, and G. F. Dresselhaus, "Raman Spectroscopy in Graphene Related Systems," ISBN 978-3-527-40811-5, 2011.

[76] A. C. Ferrari and J. Robertson, "Interpretation of Raman spectra of disordered and amorphous carbon," *Phys. Rev. B*, vol. 61, pp. 14095–14107, 2000.

[77] X. Dong, D. Fu, W. Fang, Y. Shi, P. Chen, L.-J. Li, "Doping single-layer graphene with aromatic molecules," *Small*, vol. 5, pp. 1422-1426, 2009.